

# WATER VAPOR AND THE DYNAMICS OF CLIMATE CHANGES

Tapio Schneider  
California Institute of  
Technology, Pasadena,  
California, USA

Paul A. O’Gorman  
Massachusetts Institute of  
Technology, Cambridge,  
Massachusetts, USA

Xavier Levine  
California Institute of  
Technology, Pasadena,  
California, USA

Water vapor is not only Earth’s dominant greenhouse gas. Through the release of latent heat when it condenses, it also plays an active role in dynamic processes that shape the global circulation of the atmosphere and thus climate. Here we present an overview of how latent heat release affects atmosphere dynamics in a broad range of climates, ranging from extremely cold to extremely warm. Contrary to widely held beliefs, atmospheric circulation statistics can change non-monotonically with global-mean surface temperature, in part because of dynamic effects of water vapor. For example, the strengths of the tropical Hadley circulation and of zonally asymmetric tropical cir-

culations, as well as the kinetic energy of extratropical baroclinic eddies, can be lower than they presently are both in much warmer climates and in much colder climates. We discuss how latent heat release is implicated in such circulation changes, particularly through its effect on the atmospheric static stability, and we illustrate the circulation changes through simulations with an idealized general circulation model. This allows us to explore a continuum of climates, constrain macroscopic laws governing this climatic continuum, and place past and possible future climate changes in a broader context.

## 1. INTRODUCTION

Water vapor is not only important for Earth’s radiative balance as the dominant greenhouse gas of the atmosphere. It is also an active player in dynamic processes that shape the global circulation of the atmosphere and thus climate. The latent heat released when atmospheric water vapor condenses and the cooling of air through evaporation or sublimation of condensate affect atmospheric circulations. Although the mechanisms are not well understood, it is widely appreciated that heating and cooling of air through phase changes of water are integral to moist convection and dynamics in the equatorial region. But that water vapor plays an active and important role in dynamics globally is less widely appreciated, and how it does so is only beginning to be investigated. For instance, there is evidence that the width of the Hadley circulation has increased over the past decades [e.g., *Hu and Fu*, 2007; *Seidel and Randel*, 2007; *Seidel et al.*, 2008], and it also increases in many simulations of climate change in response to increased concentrations of greenhouse

gases [e.g., *Kushner et al.*, 2001; *Lu et al.*, 2007; *Previdi and Liepert*, 2007; *Johanson and Fu*, 2009]. This widening of the Hadley circulation is often linked to the decrease in the moist-adiabatic temperature lapse rate with increasing surface temperature, which results in an increased tropical static stability and can lead to a widening of the Hadley circulation, at least in dry atmospheres [e.g., *Held*, 2000; *Walker and Schneider*, 2006; *Frierson et al.*, 2007b; *Korty and Schneider*, 2008]. Yet it is unclear how the width of the Hadley circulation in an atmosphere in which water vapor is dynamically active relates to the static stability, or in fact, how the static stability thought to be relevant—that at the subtropical termini of the Hadley circulation—is controlled.

Here we present an overview of dynamic effects of water vapor in the global circulation of the atmosphere and in climate changes. What may be called water vapor kinematics—the study of the distribution of water vapor given the motions of the atmosphere—has recently been reviewed by *Held and Soden* [2000], *Pierrehumbert et al.* [2007], and *Sherwood et al.* [2009]. We bracket off questions of water vapor kinematics to the

extent possible and instead focus on what may be called water vapor dynamics—the study of the dynamic effects of heating and cooling of air through phase changes of water.

Our emphasis lies on large scales, from the scales of extratropical storms ( $\sim 1000$  km) to the planetary scale of the Hadley circulation. In motions on such large scales, the release of latent heat through condensation generally is more important than the cooling of air through evaporation or sublimation of condensate: The residence times of vapor and condensate are similar (days and longer), and so are the specific latent heat of vaporization and that of sublimation, but the atmosphere in the global mean contains about 250 times more water vapor ( $\sim 25 \text{ kg m}^{-2}$ ) than liquid water and ice ( $\sim 0.1 \text{ kg m}^{-2}$ ) [Trenberth and Smith, 2005]. Nonetheless, even motions on large scales are affected by smaller-scale dynamics such as moist convection, for which cooling through evaporation of condensate and the convective downdrafts thereby induced are essential [e.g., Emanuel *et al.*, 1994]. The emphasis on large scales allows us to sideline some of the complexities of moist convection and consider only the collective effect of many convective cells on their large-scale environment, assuming that the convective cells adjust rapidly to their environment and so are in statistical equilibrium (“quasi-equilibrium”) with it [Arakawa and Schubert, 1974]. Our reasoning about the effect of moist convection on large-scale motions builds upon the cornerstone of convective quasi-equilibrium dynamics, well supported by observations and simulations of radiative-convective equilibrium: convection, where it occurs, tends to establish a thermal stratification with moist-adiabatic temperature lapse rates (see Emanuel *et al.* [1994], Emanuel [2007], and Neelin *et al.* [2008] for overviews).

Dynamic effects of water vapor in the global circulation of the atmosphere have typically been discussed in the context of specific past climates, such as that of the Last Glacial Maximum (LGM), or possible future climate changes in response to increased concentrations of greenhouse gases. We view past and possible future climates as parts of a climatic continuum that is governed by universal, albeit largely unknown, macroscopic laws. Our goal is to constrain the forms such macroscopic laws may take. They cannot be inferred from observational data, as it can be misleading to infer laws governing climate changes from fluctuations within the present climate (e.g., from El Niño and the Southern Oscillation, as we will discuss further below). And they are difficult to infer from simulations with comprehensive climate models, whose complexity can obscure the chain of causes and effects in climate changes.

Therefore, we illustrate theoretical developments in what follows with simulations of a broad range of climates with an idealized general circulation model

(GCM). The simulations are described in detail in O’Gorman and Schneider [2008a]. They are made with a GCM similar to that of Frierson *et al.* [2006], containing idealized representations of dynamic effects of water vapor but not accounting for complexities not directly related to water vapor dynamics. For example, the GCM has a surface that is uniform and water covered (a “slab ocean” that does not transport heat), and there are no topography and no radiative water vapor or cloud feedbacks. The GCM employs a variant of the quasi-equilibrium moist convection scheme of Frierson [2007], has insolation fixed at perpetual equinox, and takes only the vapor-liquid phase transition of water into account, assuming a constant specific latent heat of vaporization. Consistently but unlike what would occur in the real world, ice is ignored in the model, be it as cloud ice, sea ice, or land ice. We obtained a broad range of statistically steady, axisymmetric, and hemispherically symmetric climates by varying the optical thickness of an idealized atmospheric longwave absorber, keeping shortwave absorption fixed and assuming gray radiative transfer. The climates have global-mean surface temperatures ranging from 259 K (pole-equator surface temperature contrast 70 K) to 316 K (temperature contrast 24 K) and atmospheric water vapor concentrations varying by almost two orders of magnitude. We will discuss dynamic effects of water vapor in past and possible future climates in the context of this broad sample from a climatic continuum, making connections to observations and more comprehensive GCMs wherever possible. This allows us to examine critically, and ultimately to reject, some widely held beliefs, such as that the Hadley circulation would generally become weaker as the climate warms, or that extratropical storms would generally be stronger than they are today in a climate like that of the LGM with larger pole-equator surface temperature contrasts.

Section 2 reviews energetic constraints on the concentration of atmospheric water vapor and precipitation as background for the discussion of how water vapor dynamics affects climate changes. Section 3 examines tropical circulations, with emphasis on the Hadley circulation. Section 4 examines extratropical circulations, with emphasis on extratropical storms and the static stability, which occupies a central place if one wants to understand the effects of water vapor on extratropical dynamics. Section 5 summarizes conclusions and open questions.

## 2. ENERGETIC CONSTRAINTS ON WATER VAPOR CONCENTRATION AND PRECIPITATION

Water vapor dynamics is more important in warmer than in colder climates because the atmospheric water vapor concentration generally increases with surface temperature. This is a consequence of the rapid increase of the saturation vapor pressure with temperature. According to the Clausius-Clapeyron relation, a

small change  $\delta T$  in temperature  $T$  leads to a fractional change  $\delta e^*/e^*$  in saturation vapor pressure  $e^*$  of

$$\frac{\delta e^*}{e^*} \approx \frac{L}{R_v T^2} \delta T, \quad (1)$$

where  $R_v$  is the gas constant of water vapor and  $L$  is the specific latent heat of vaporization. If one substitutes temperatures representative of near-surface air in the present climate, the fractional increase in saturation vapor pressure with temperature is about 6–7% K<sup>-1</sup>, that is, the saturation vapor pressure increases 6–7% if the temperature increases 1 K (e.g., *Boer* [1993]; *Wentz and Schabel* [2000]; *Held and Soden* [2000]; *Trenberth et al.* [2003]). In Earth's atmosphere in the past decades, precipitable water (column-integrated specific humidity) has varied with surface temperature at a rate of 7–9% K<sup>-1</sup>, averaged over the tropics or over all oceans [*Wentz and Schabel*, 2000; *Trenberth et al.*, 2005]. Thus, the fractional variations in precipitable water are similar to those in near-surface saturation vapor pressure. They are consistent with an approximately constant effective relative humidity—the ratio of column-integrated vapor pressure to saturation vapor pressure, or the relative-humidity average weighted by the saturation vapor pressure, i.e., weighted toward the lower troposphere. Similarly, in simulations of climate change scenarios, global-mean precipitable water increases with global-mean surface temperature at a rate of  $\sim 7.5\%$  K<sup>-1</sup>, likewise consistent with an approximately constant effective relative humidity [*Held and Soden*, 2006; *Willett et al.*, 2007; *Stephens and Ellis*, 2008].

But global-mean precipitation and evaporation (which are equal in a statistically steady state) increase more slowly with temperature than does precipitable water. In simulations of climate change scenarios, global-mean precipitation and evaporation increase with global-mean surface temperature at a rate of only 2–3% K<sup>-1</sup>—considerably less than the rate at which precipitable water increases [e.g., *Knutson and Manabe*, 1995; *Allen and Ingram*, 2002; *Held and Soden*, 2006; *Stephens and Ellis*, 2008]. They have varied with surface temperature at a similar rates in Earth's atmosphere in the past decades [*Adler et al.*, 2008]. This points to energetic constraints on the global-mean precipitation and evaporation [*Boer*, 1993].

The surface energy balance closely links changes in evaporation to changes in near-surface saturation specific humidity and relative humidity. The evaporation  $E$  enters the surface energy balance as the latent heat flux  $LE$ , which, in Earth's present climate, is the largest loss term balancing the energy gained at the surface through absorption of solar radiation [*Kiehl and Trenberth*, 1997; *Trenberth et al.*, 2009]. The evaporation is related to the specific humidity  $q$  near the surface and the saturation specific humidity  $q_s^*$  at the surface by the bulk aerodynamic formula,

$$E \approx \rho C_W \|\mathbf{v}\| (q_s^* - q). \quad (2)$$

Here,  $\rho$  is the density of near-surface air,  $\mathbf{v}$  is the near-surface wind,  $C_W$  is a bulk transfer coefficient, and the formula is valid over oceans, where most evaporation occurs (e.g., *Peixoto and Oort* [1992]). Over oceans, the disequilibrium factor  $q_s^* - q$  between the surface and near-surface air is usually dominated by the subsaturation of near-surface air, rather than by the temperature difference between the surface and near-surface air; therefore, it can be approximated as  $q_s^* - q \approx (1 - \mathcal{H})q_s^*$ , with near-surface relative humidity  $\mathcal{H}$ . Changes in near-surface relative humidity  $\delta \mathcal{H}$  can then be related to fractional changes in evaporation  $\delta E/E$  and near-surface saturation specific humidity  $\delta q_s^*/q_s^*$  if we make two simplifying assumptions: (i) changes in evaporation with climate are dominated by changes in the disequilibrium factor  $q_s^* - q$ , and (ii) changes in the disequilibrium factor  $q_s^* - q$ , in turn, are dominated by changes in near-surface relative humidity and saturation specific humidity, so that  $\delta(q_s^* - q) \approx (1 - \mathcal{H})\delta q_s^* - q_s^*\delta \mathcal{H}$ . This leads to

$$\delta \mathcal{H} \approx (1 - \mathcal{H}) \left( \frac{\delta q_s^*}{q_s^*} - \frac{\delta E}{E} \right), \quad (3)$$

an expression equivalent to one used by *Boer* [1993] to evaluate hydrologic-cycle changes in climate change simulations.

As discussed by *Boer* [1993] and *Held and Soden* [2000], the relation (3) together with the surface energy balance constrain the changes in evaporation and near-surface relative humidity that are possible for a given change in radiative forcing and temperature. Assume evaporation increases with surface temperature at 2.5% K<sup>-1</sup> in the global mean, and saturation vapor pressure increases at 6.5% K<sup>-1</sup>, as it does in typical climate change simulations. Then, if the global-mean surface temperature increases by 3 K, the global-mean evaporation increases by  $\delta E/E \approx 7.5\%$ , and the saturation specific humidity at the surface increases by  $\delta q_s^*/q_s^* \approx \delta e^*/e^* \approx 19.5\%$ . To the extent that the relation (3) is adequate and for a near-surface relative humidity of 80%, it follows that the relative humidity  $\mathcal{H}$  increases by about  $\delta \mathcal{H} = (1 - 0.8)(19.5 - 7.5) = 2.4$  percentage points—a comparatively small change. The precise magnitude of the relative humidity changes depends on changes in the surface winds and in the temperature difference between the surface and near-surface air. However, even if, for example, changes in the temperature difference between the surface and near-surface air influence the disequilibrium factor  $q_s^* - q$  similarly strongly as changes in the near-surface relative humidity, the order of magnitude of the terms shows that the near-surface relative humidity generally changes less than the near-surface saturation specific humidity. This is especially the case if the near-surface air is close to saturation, so that the factor  $(1 - \mathcal{H})$  in (3) is small.

Because most water vapor in the atmosphere is confined near the surface (the water vapor scale height is

$\sim 2$  km), the fact that changes in near-surface relative humidity are constrained to be relatively small implies that changes in precipitable water are dominated by changes in the near-surface saturation specific humidity. Hence, precipitable water changes scale approximately with the rate given by the Clausius-Clapeyron relation (1), as seen in observed climate variations and simulated climate change scenarios. Free-tropospheric relative humidity need not stay fixed, however, so precipitable water changes may deviate slightly from Clausius-Clapeyron scaling.

It is also clear that the rate of change of evaporation with global-mean surface temperature cannot differ vastly from the  $2\text{--}3\% \text{ K}^{-1}$  quoted above, as would be necessary for significant relative humidity changes. To illustrate how strongly changes in evaporation and near-surface relative humidity are constrained by the surface energy balance, consider a hypothetical case that will turn out to be impossible: assume an increase in the concentration of greenhouse gases would lead to a 3-K global-mean surface temperature increase in a sta-

tistically steady state, accompanied by a global-mean saturation specific humidity increase at the surface by  $\sim 19.5\%$ ; assume further that this would lead to a reduction in near-surface relative humidity from 80% to 70%. According to (3), evaporation would then have to increase by  $\sim 70\%$  in the global mean. Currently total evaporation at Earth's surface amounts to a latent heat flux of about  $80 \text{ W m}^{-2}$  [Kiehl and Trenberth, 1997; Trenberth et al., 2009]. A 70% increase would imply that an additional energy flux of  $56 \text{ W m}^{-2}$  would have to be available to the surface to balance the additional evaporation. The global-mean net irradiance would have to increase and/or the upward sensible heat flux at the surface would have to decrease by this amount. But this is impossible: Current estimates of the equilibrium climate sensitivity are of order  $0.8 \text{ K}$  surface warming per  $1 \text{ W m}^{-2}$  radiative forcing at the top of the atmosphere, and the radiative forcing at the surface can be of the same order as that at the top of the atmosphere (though they are generally not equal). So a 3-K global-mean surface temperature increase is inconsistent with a  $56 \text{ W m}^{-2}$  increase in net irradiance at the surface. Likewise, the upward sensible heat flux cannot decrease sufficiently to provide the additional energy flux at the surface because it amounts to only about  $20 \text{ W m}^{-2}$  in the global mean and  $10 \text{ W m}^{-2}$  in the mean over oceans, where most evaporation occurs [Kiehl and Trenberth, 1997; Trenberth et al., 2009]. The implication of these order-of-magnitude arguments is that changes in near-surface relative humidity and in evaporation—and thus, in a statistically steady state, in global-mean precipitation—are strongly energetically constrained. Order-of-magnitude estimates of the climate sensitivity indicate global-mean evaporation can change by  $O(2\% \text{ K}^{-1})$ , and the relation (3) then implies that the near-surface relative humidity can change by  $O(1\% \text{ K}^{-1})$  or less.

The expectations based on the energetic arguments are borne out in the idealized GCM simulations mentioned in the introduction and described in O’Gorman and Schneider [2008a]. Over a broad range of climates and in the global mean, precipitable water increases exponentially with surface temperature, roughly at the same rate as the column-integrated saturation specific humidity, which is dominated by near-surface contributions (Fig. 1a). The effective relative humidity varies little with climate, compared with the variations in precipitable water by almost two orders of magnitude. Nonetheless, the effective relative humidity is not exactly constant but increases by about 5 percentage points from the colder to the warmer simulations (if the stratosphere is excluded from the calculation of the column-integrated saturation specific humidity, otherwise the increase is larger, and it generally is sensitive to precisely how it is calculated). The increase in the effective relative humidity is qualitatively consistent with the relation (3), which implies an increase in the near-surface relative humidity if the fractional

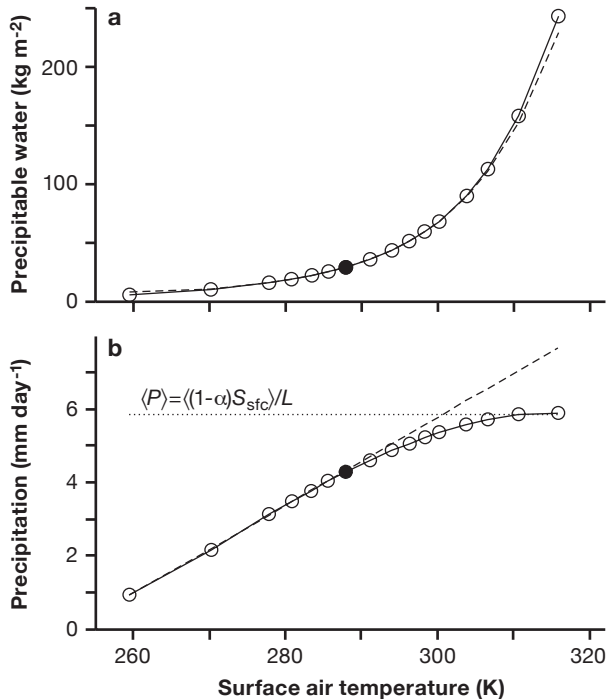


**Figure 1.** Global-mean precipitable water and precipitation vs global-mean surface temperature in idealized GCM simulations. Each circle represents a statistically steady state of a GCM simulation. The filled circle marks a reference simulation with a climate resembling that of present-day Earth. (a) Precipitable water. The dashed line is the global-mean column-integrated saturation specific humidity, calculated excluding levels in the upper atmosphere (pressures  $\lesssim 0.05 \text{ hPa}$ ) and rescaled by a constant effective relative humidity factor of 0.67. In the idealized GCM, the specific latent heat of vaporization is taken to be constant, and the saturation specific humidity is calculated consistently with this approximation. (b) Precipitation. The dashed line shows the approximate upper bound (1). (Adapted from O’Gorman and Schneider [2008a].)

increase in saturation specific humidity exceeds that in evaporation, as it does in all but the coldest simulations. However, the energetic arguments only constrain the near-surface relative humidity, not the relative humidity of the free troposphere. The latter varies substantially among the simulations. For example, in the extratropical free troposphere, the relative humidity decreases by more than 15 percentage points from the coldest to the warmest simulation [O’Gorman and Schneider, 2008a, their Fig. 1]. The relative humidity also changes more strongly in the free troposphere than near the surface in simulations of climate change scenarios with comprehensive GCMs [Lorenz and DeWeaver, 2007]. Contrary to what is sometimes surmised, there is no universal principle that constrains free-tropospheric relative humidity changes to be negligible or even to be of the same sign as near-surface relative humidity changes. This implies in particular that the energetic arguments alone do not constrain the strength of the radiative water vapor feedback, which is sensitive to the free-tropospheric specific humidity [e.g., Held and Soden, 2000].

In cold and moderately warm simulations, precipitation increases roughly linearly with surface temperature in the global mean and asymptotes to an approximately constant value in the warmest simulations (Fig. 1b). Precipitation generally increases more slowly with surface temperature than does precipitable water, except in the coldest simulations. For example, at the reference simulation with global-mean surface temperature closest to that of present-day Earth (288 K, filled circle in Fig. 1), precipitable water increases at  $6.2\% \text{ K}^{-1}$  in the global mean, whereas precipitation increases at only  $2.5\% \text{ K}^{-1}$ . It is unclear why precipitation increases roughly linearly with surface temperature over a wide range of climates; energetic constraints appear to play a role [O’Gorman and Schneider, 2008a]. The constant value to which the precipitation asymptotes is that at which the solar radiation absorbed at the surface approximately balances the latent heat flux and thus evaporation and precipitation in the global mean,

$$\langle P \rangle_{\text{max}} \approx \langle (1 - \alpha) S_{\text{sfc}} \rangle / L. \quad (4)$$

Here,  $\langle \cdot \rangle$  denotes a global mean;  $\alpha$  is the surface albedo and  $S_{\text{sfc}}$  the downwelling solar radiative flux at the surface, which both are fixed in our idealized GCM simulations (in reality they would vary with climate because, e.g., the cloud albedo and the absorption of solar radiation by water vapor would vary). In fact, the global-mean precipitation exceeds the value (1) slightly in the warmest simulations because in warm climates there is a net sensible heat flux from the atmosphere to the surface [Pierrehumbert, 2002]. The sensible heat flux adds to the absorbed solar irradiance in providing energy available to evaporate water. (The net of the upwelling and downwelling longwave radiative fluxes

is small in the warmest simulations with atmospheres that are optically thick for longwave radiation.)

The simulation results make explicit how the energy balance constrains changes in precipitable water and precipitation. It should be borne in mind that the energetic arguments constrain only the relative humidity near the surface, not in the free atmosphere, and only the global-mean precipitation and evaporation, not local precipitation, which is influenced by transport of water vapor in the atmosphere. Local precipitation may increase more rapidly with surface temperature than global-mean precipitation, as may have happened in the past decades over parts of the tropics (e.g., over oceans) [Gu et al., 2007; Allan and Soden, 2007]. However, reports that global precipitation and evaporation increase much more rapidly with surface temperature than stated here [e.g., Wentz et al., 2007] have to be regarded with caution; they may be affected by measurement and analysis errors and uncertainties resulting from estimating trends from noisy time series [see also Adler et al., 2008; Stephens and Ellis, 2008].

### 3. TROPICAL CIRCULATIONS

#### 3.1. Gross Upward Mass Flux

That global-mean precipitable water and precipitation change with climate at different rates has one immediate consequence: the water vapor cycling rate—the ratio of global-mean precipitation and precipitable water—changes. Global-mean precipitation increases more slowly with surface temperature than does global-mean precipitable water for all but the two coldest idealized GCM simulations. Hence, the water vapor cycling rate decreases with surface temperature for all but the two coldest simulations, from more than  $0.15 \text{ day}^{-1}$  in the colder simulations to less than  $0.025 \text{ day}^{-1}$  in the warmest simulations (Fig. 2). At the reference simulation, the water vapor cycling rate decreases with

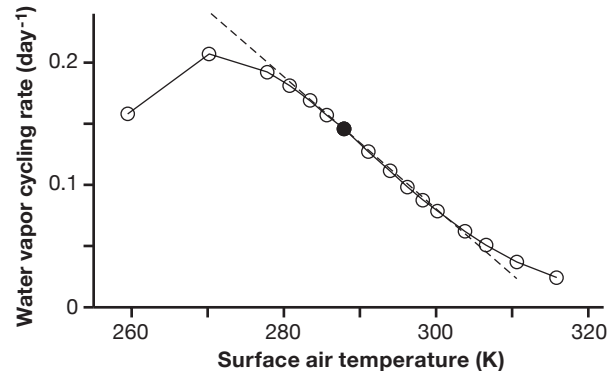


**Figure 2.** Water vapor cycling rate vs global-mean surface temperature in idealized GCM simulations. The cycling rate is the ratio of global-mean precipitation (Fig. 1b) and precipitable water (Fig. 1a, up to a factor of water density). The dashed line marks a decrease of cycling rate of  $3.7\% \text{ K}^{-1}$  relative to the reference simulation (filled circle).



global-mean surface temperature at  $3.7\% \text{ K}^{-1}$ , the difference between the rates of increase in precipitation ( $2.5\% \text{ K}^{-1}$ ) and precipitable water ( $6.2\% \text{ K}^{-1}$ ). The water vapor cycling rate decreases at similar rates in simulations of climate change scenarios with comprehensive GCMs [e.g., *Knutson and Manabe*, 1995; *Roads et al.*, 1998; *Bosilovich et al.*, 2005; *Held and Soden*, 2006; *Stephens and Ellis*, 2008]. A decreasing water vapor cycling rate may be interpreted as a weakening of the atmospheric water cycle and may imply a weakening of the atmospheric circulation, particularly in the tropics where most of the water vapor is concentrated and precipitation is maximal [e.g., *Betts and Ridgway*, 1989; *Betts*, 1998; *Held and Soden*, 2006; *Vecchi et al.*, 2006; *Vecchi and Soden*, 2007].

A more precise relation between precipitation, specific humidity, and the gross upward (convective) mass flux in the tropics follows from considerations of the water vapor budget. In updrafts in the tropical troposphere, above the lifted condensation level where the updraft air is saturated with water vapor, the dominant balance in the water vapor budget is between vertical advection of water vapor and condensation. That is,

$$-\omega^\uparrow \partial_p q^* \approx c, \quad (5)$$

where  $q^*$  is the saturation specific humidity,  $c$  is the condensation rate, and

$$\omega^\uparrow = \begin{cases} \omega & \text{if } \omega < 0 \\ 0 & \text{if } \omega \geq 0 \end{cases} \quad (6)$$

is the upward component of the vertical velocity  $\omega = Dp/Dt$  in pressure coordinates. Integrating in the vertical yields a relation between the upward velocity, precipitation, and saturation specific humidity,

$$-\{\omega^\uparrow \partial_p q^*\} \approx P, \quad (7)$$

where  $\{\cdot\} = g^{-1} \int dp(\cdot)$  denotes the mass-weighted vertical integral over an atmospheric column [cf. *Iribarne and Godson*, 1981, chapter 9.14]. We have assumed that the vertically integrated condensation rate is approximately equal to the precipitation rate,  $\{c\} \approx P$ , which means that we have neglected evaporation or sublimation of condensate. This is justifiable if the relation (7) is understood as applying to horizontal averages over convective systems, such that the upward velocity  $\omega^\uparrow$  is the net upward velocity within convective systems—the net of convective updrafts and convective downdrafts induced by evaporation or sublimation of condensate. When understood in this way, the relation (7) holds instantaneously, not only in long-term averages, and can be used, for example, to relate precipitation extremes to updraft velocities and thermodynamic conditions, even in the extratropics [*O’Gorman and Schneider*, 2009a, b].

From the relation (7), one can obtain different scaling estimates that give qualitatively different predictions of how the tropical gross upward mass flux changes with

climate. If the bulk of the condensation occurs between a near-surface level with saturation specific humidity  $q_s^*$  and some tropospheric level with saturation specific humidity  $q^*$ , the gross upward mass flux scales as

$$-\frac{\omega^\uparrow}{g} \sim \frac{P}{\Delta q^*}, \quad (8a)$$

where  $\Delta q^* = q_s^* - q^*$ . This scaling estimate was suggested by *Betts* [1998], based on the radiative-convective equilibrium model of *Betts and Ridgway* [1989]. If one follows these authors or *Held and Soden* [2006] further and assumes that the relevant tropospheric saturation specific humidity  $q^*$  either is negligible or scales linearly with the near-surface saturation specific humidity  $q_s^*$ , the estimate (8a) simplifies to

$$-\frac{\omega^\uparrow}{g} \sim \frac{P}{q_s^*}. \quad (8b)$$

To the extent that global-mean precipitation and precipitable water scale with the tropical precipitation and near-surface saturation specific humidity (which is not guaranteed), this scaling estimate implies that the tropical gross upward mass flux scales with the water vapor cycling rate, as suggested by *Held and Soden* [2006].

The scaling estimates (8a) and (8b) for the gross upward mass flux can differ substantially because the saturation specific humidity contrast  $\Delta q^*$  generally increases less rapidly with temperature than the saturation specific humidity  $q^*$ . For example, if the ther-

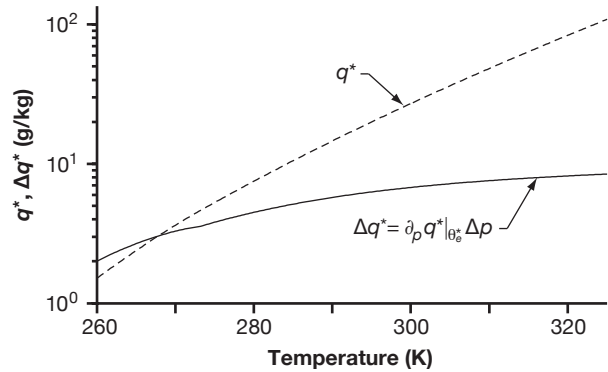


**Figure 3.** Saturation specific humidity  $q^*$  and saturation specific humidity contrast  $\Delta q^* = \partial_p q^*|_{\theta_c} \Delta p$  as a function of temperature. Both are evaluated at 825 hPa, and the pressure difference  $\Delta p = 250$  hPa is taken to be fixed. The saturation specific humidity is calculated according to the modified Tetens formula given in *Simmons et al.* [1999], using the saturation vapor pressure over ice at very low temperatures, that over liquid water at temperatures above the freezing point, and a quadratic interpolation between the two at intermediate (mixed-phase) temperatures below the freezing point. (That is, freezing of water is taken into account in this figure, in contrast to the idealized GCM simulations, in which only the vapor-liquid phase transition is taken into account.) The fractional rate of increase of  $q^*$  varies between 9.5 and 5.2%  $\text{K}^{-1}$  from low to high temperatures in the range shown, and that of  $\Delta q^*$  varies between 6.6 and 0.6%  $\text{K}^{-1}$ . Note the logarithmic scale of the ordinate.

mal stratification in convective systems is moist adiabatic, the saturation specific humidity contrast may scale as  $\Delta q^* \sim \partial_p q^*|_{\theta_e^*} \Delta p$ , where the saturation specific humidity derivative is taken along a moist adiabat with constant equivalent potential temperature  $\theta_e^*$ , and the pressure difference  $\Delta p$  is taken to be fixed [Betts and Harshvardhan, 1987; O’Gorman and Schneider, 2009a, b]. The saturation specific humidity contrast  $\Delta q^*$  then scales with the moist-adiabatic static stability  $S^* = -(T/\theta) \partial_p \theta|_{\theta_e^*}$  (potential temperature  $\theta$ ) because on a moist adiabat, adiabatic cooling balances diabatic heating through latent heat release, so that the static stability and saturation specific humidity derivative are related by  $S^* \approx (L/c_p) \partial_p q^*|_{\theta_e^*}$  [e.g., Iribarne and Godson, 1981, chapter 7.8]. Now, the saturation specific humidity contrast  $\Delta q^*$  generally increases with temperature at a smaller fractional rate than the saturation specific humidity  $q^*$ , with the difference between the rates increasing with temperature (Fig. 3). At a temperature and pressure typical of the tropical lower troposphere in the present climate (290 K and 825 hPa),  $\Delta q^*$  increases with temperature at  $2.0\% \text{ K}^{-1}$ , while  $q^*$  increases at  $6.4\% \text{ K}^{-1}$ . A fractional increase in tropical precipitation of  $2.5\% \text{ K}^{-1}$  (relative to a lower-tropospheric temperature) would imply a change in the gross upward mass flux of  $(2.5 - 2.0)\% \text{ K}^{-1} = 0.5\% \text{ K}^{-1}$  according to the estimate (8a) but of  $(2.5 - 6.4)\% \text{ K}^{-1} = -3.9\% \text{ K}^{-1}$  according to the estimate (8b). Thus, the differences between the two estimates can imply changes in the gross upward mass flux of opposite sign: slight strengthening according to (8a) and weakening according to (8b). Both estimates are based on rough scaling assumptions,

and neither may be very accurate (e.g., the relevant pressure difference  $\Delta p$  is not necessarily fixed but may vary with climate). But they illustrate that the gross upward mass flux does not necessarily scale with the water vapor cycling rate and may depend, for example, on the vertical profile of the upward velocity (averaged over convective systems, that is, including contributions from convective downdrafts).

We test the scaling estimates for the tropical gross upward mass flux using the upward mass flux on the idealized GCM’s grid scale, sampled four times daily, as a proxy for the unresolved subgrid-scale convective mass flux.<sup>1</sup> We have verified that the grid-scale upward mass flux satisfies relation (7), so that any errors in the scaling estimates are due to the assumptions made in the estimates. Integrating the grid-scale upward mass flux over an equatorial latitude band gives

$$\Psi^\uparrow(\phi, p) = -\frac{2\pi a^2}{g} \int_0^\phi \bar{\omega}^\uparrow(\phi', p) \cos \phi' d\phi', \quad (9)$$

where  $a$  is Earth’s radius,  $\phi$  is latitude, and the overbar denotes a zonal and temporal mean along isobars. With these conventions, the integrated gross upward mass flux  $\Psi^\uparrow$  is directly comparable with the (net) mass transport streamfunction  $\Psi$ , which, because the simulations are statistically symmetric about the equator, is obtained by replacing the upward velocity  $\omega^\uparrow$  in (9) with the net vertical velocity  $\omega$ . Figure 4 shows  $\Psi^\uparrow$  and  $\Psi$  evaluated at  $4^\circ$  latitude and at a pressure<sup>2</sup> of approximately 825 hPa (i.e., it shows mass fluxes across the 825-hPa level integrated between the equator and  $4^\circ$ ). The 825-hPa level is in all simulations within  $\lesssim 50$  hPa of the level at which the gross upward mass flux is maximal and at which the condensation in the column can be expected to be maximal. (The level of maximum gross upward mass flux likely depends on specifics of the convection and radiation parameterization and so may be different in other GCMs.) The figure also shows the estimates  $\hat{\Psi}_a^\uparrow$  and  $\hat{\Psi}_b^\uparrow$  for the integrated gross upward mass flux that are obtained by substituting the scaling estimates (8a) and (8b) for the upward mass flux  $-\omega^\uparrow/g$  in (9). We evaluate the near-surface saturation specific humidity  $q_s^*$  at 950 hPa and the tropospheric saturation specific humidity  $q^*$  at 700 hPa—levels chosen to fit the estimates to the actual gross upward mass flux as closely as possible. It is evident that the estimate  $\hat{\Psi}_b^\uparrow$  overestimates the changes in the gross upward mass flux. The water vapor cycling rate in Fig. 2 scales similarly to the estimate  $\hat{\Psi}_b^\uparrow$ , so it likewise is not a good estimate of the gross upward mass flux. The estimate  $\hat{\Psi}_a^\uparrow$  gives a better fit. At the reference simulation, the gross upward mass flux decreases with global-mean surface temperature at about  $1\% \text{ K}^{-1}$ —more slowly by a factor  $\sim 3$  than the estimate  $\hat{\Psi}_b^\uparrow$  or the water vapor cycling rate, and roughly consistent with the moist-adiabatic static stability arguments and the estimate  $\hat{\Psi}_a^\uparrow$  (Fig. 3).

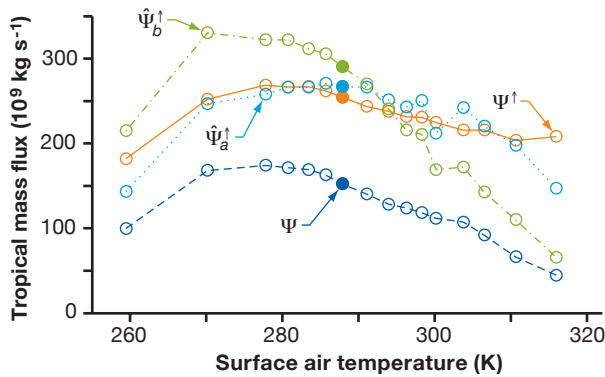


**Figure 4.** Tropical vertical mass flux and scaling estimates vs global-mean surface temperature in idealized GCM simulations. Shown are the integrated gross upward mass flux  $\Psi^\uparrow$ , the mass transport streamfunction  $\Psi$ , and the scaling estimates  $\hat{\Psi}_a^\uparrow$  and  $\hat{\Psi}_b^\uparrow$  corresponding to Eqs. (8a) and (8b), all evaluated at  $4^\circ$  latitude and at a pressure of approximately 825 hPa and averaged over both, statistically identical, hemispheres. The scaling estimates  $\hat{\Psi}_a^\uparrow$  and  $\hat{\Psi}_b^\uparrow$  are multiplied by constants (2.6 and 1.6, respectively) that are chosen such that the mean-square deviation between the scaling estimate and the integrated gross upward mass flux  $\Psi^\uparrow$  is minimized.

The simulations demonstrate that at least in this idealized GCM, to understand changes in the gross upward mass flux, it is important to consider not just changes in the near-surface saturation specific humidity but changes in the saturation specific humidity stratification, or in the static stability—as did, for example, *Knutson and Manabe* [1995]. The corresponding scaling estimates are clearly distinguishable. They not only imply quantitatively different rates at which the gross upward mass flux changes with climate; they can also imply qualitatively different results in that their maxima occur in different climates (Fig. 4). Because the gross upward mass flux in the tropics represents the bulk of the global gross upward mass flux, similar conclusions to those drawn here for the tropics also apply to the global mean.

The gross upward mass flux in Earth's tropical atmosphere appears to have decreased as the climate warmed in recent decades [*Tanaka et al.*, 2004; *Vecchi et al.*, 2006; *Zhang and Song*, 2006]. These observations are consistent with the idealized GCM simulations, in which the gross upward mass flux in the tropics exhibits a maximum at a climate somewhat colder than that of the present day. By how much the gross upward mass flux in Earth's tropical atmosphere flux has decreased, however, is difficult to ascertain because of data uncertainties. In simulations of climate change scenarios, the gross upward mass flux also decreases as the surface temperature increases, both globally and in the tropics, with most of the decrease in the tropics occurring in zonally asymmetric circulation components (e.g., in the Walker circulation), not in the zonal-mean Hadley circulation [*Held and Soden*, 2006]. The gross upward mass flux decreases more slowly than the water vapor cycling rate in almost all models used in the IPCC Fourth Assessment Report [*Vecchi and Soden*, 2007]. *Vecchi and Soden* [2007] interpreted this result as being roughly consistent with the scaling of the gross upward mass flux with the water vapor cycling rate and speculated that non-precipitating upward mass fluxes are responsible for the systematic deviations from this scaling. However, their results appear more consistent with our idealized GCM simulations and with the assumption that the saturation specific humidity stratification, rather than the water vapor cycling rate, is important for the scaling of the gross upward mass flux.<sup>3</sup>

Thus, in climates similar to the present or warmer, the gross upward mass flux in the tropics likely decreases as the climate warms. Convective activity, by this bulk measure, likely decreases as the climate warms—which may seem counterintuitive because it generally increases with surface temperature (or near-surface specific humidity) when spatial or temporal fluctuations within the present climate are considered. The reason for the different responses is that water vapor dynamics plays different roles in climate changes and in fluctuations within a given climate. As the climate

warms, when surface temperatures increase on large scales, large-scale precipitation changes are energetically constrained, latent heat release in moist convection increases the large-scale tropical static stability (the moist-adiabatic lapse rate decreases), and both effects together can lead to a weakening of the gross upward mass flux [*Betts*, 1998]. In fluctuations within a given climate, the static stability is controlled by processes on large scales, and latent heat release can locally induce potentially strong upward mass fluxes. This illustrates how misleading it can be to use fluctuations within the present climate (such as El Niño and the Southern Oscillation) for inferences about climate changes. For example, while observations suggest that there may be a threshold sea surface temperature that must be exceeded for strong convection to occur over Earth's tropical oceans [e.g., *Graham and Barnett*, 1987; *Folkins and Braun*, 2003], there is no justification for using the same threshold temperature for inferences about convection in changed climates: to the extent that such a threshold temperature exists, it may change as the climate changes, and with it the large-scale tropical static stability [e.g., *Knutson and Manabe*, 1995; *Neelin et al.*, 2009].

Our focus has been on integrated measures of the gross upward mass flux, which are constrained by large-scale energetic and hydrologic balances. Regionally, the response to climate changes is less constrained and can be more complex. For example, margins of convective regions are particularly susceptible to relatively large changes in upward mass fluxes and precipitation [e.g., *Neelin et al.*, 2003; *Chou and Neelin*, 2004; *Neelin et al.*, 2006; *Neelin*, 2007; *Chou et al.*, 2009].

### 3.2. Strength of Hadley Circulation

While arguments based on energetic and hydrologic balances alone constrain how the tropical gross upward mass flux changes with climate, they are generally insufficient to constrain how the net vertical mass flux and thus the strength of the Hadley circulation change. Even near the equator, within the ascending branch of the Hadley circulation, the net vertical mass flux amounts to only a fraction of the gross upward mass flux. For example, in the idealized GCM simulations, the gross upward mass flux  $\Psi^\uparrow$  in the lower troposphere, integrated over an equatorial latitude band within the ascending branch of the Hadley circulation, is a factor 2–5 larger than the corresponding net vertical mass flux  $\Psi$  (Fig. 4). This means that even in this equatorial latitude band, 1/2 to 4/5 of the upward mass fluxes is offset by downward mass fluxes between the (parameterized) convective systems in which the upward mass fluxes occur. In the idealized GCM simulations, the net vertical mass flux  $\Psi$  scales similarly to the gross upward mass flux  $\Psi^\uparrow$ , except in the warmest simulations (Fig. 4), but this is not generally so; we have obtained simulations with an idealized GCM containing a repre-



sensation of ocean heat transport in which the two mass fluxes scale differently over a broad range of climates.

The reason why the strength of the Hadley circulation responds differently to climate changes than the gross upward mass flux is that the Hadley circulation is not only constrained by energetic and hydrologic balances but also by the angular momentum balance, which it must obey irrespective of water vapor dynamics. In the upper troposphere above the center of the Hadley cells—where frictional processes and the vertical advection of momentum by the mean meridional circulation are negligible—the mean balance of angular momentum about Earth’s spin axis in a statistically steady state is approximately

$$(f + \bar{\zeta})\bar{v} = f(1 - \text{Ro})\bar{v} \approx \mathcal{S}. \quad (10)$$

Here,  $\text{Ro} = -\bar{\zeta}/f$  is a spatially varying local Rossby number with Coriolis parameter  $f$  and relative vorticity  $\zeta$ ,  $v$  is the meridional velocity, and  $\mathcal{S}$  is the eddy (angular) momentum flux divergence [Schneider, 2006; Walker and Schneider, 2006]. The Hadley circulation conserves angular momentum in its upper branch in the limit  $\text{Ro} \rightarrow 1$  and  $\mathcal{S} \rightarrow 0$ , in which the angular momentum or zonal momentum balance (10) degenerates and provides no constraint on the mean meridional mass flux ( $\propto \bar{v}$ ). Only in this limit does the Hadley circulation strength respond directly to changes in thermal driving [cf. Held and Hou, 1980]. In the limit  $\text{Ro} \rightarrow 0$ , the Hadley circulation strength ( $\propto \mathcal{S}/f$ ) responds to climate changes only via changes in the eddy momentum flux divergence  $\mathcal{S}$ , and possibly via changes in the width of the Hadley cells that can affect the relevant value of the Coriolis parameter  $f$  near their center. In

this limit, changes in thermal driving affect the Hadley circulation strength only insofar as they affect the eddy momentum flux divergence  $\mathcal{S}$  or the relevant value of the Coriolis parameter  $f$ . The local Rossby number  $\text{Ro}$  above the center of a Hadley cell is a nondimensional measure of how close the upper branch is to the angular momentum-conserving limit. In the limit  $\text{Ro} \rightarrow 1$ , nonlinear momentum advection by the mean meridional circulation,  $f\text{Ro}\bar{v} = \bar{v}(a \cos \phi)^{-1} \partial_\phi(\bar{u} \cos \phi)$ , dominates over eddy momentum flux divergence. In the limit  $\text{Ro} \rightarrow 0$ , eddy momentum flux divergence dominates over nonlinear momentum advection by the mean meridional circulation.

For intermediate local Rossby numbers  $0 < \text{Ro} < 1$ , the Hadley circulation strength can respond to climate changes both via changes in the eddy momentum flux divergence and via changes in the local Rossby number. The zonal momentum balance (10) implies that a small fractional change  $\delta\bar{v}/\bar{v}$  in the strength of the upper-tropospheric mean meridional mass flux must be met by changes in the eddy momentum flux divergence,  $\delta\mathcal{S}$ , in the local Rossby number,  $\delta\text{Ro}$ , and in the relevant value of the Coriolis parameter,  $\delta f$ , satisfying

$$\frac{\delta\bar{v}}{\bar{v}} \approx \frac{\delta\mathcal{S}}{\mathcal{S}} + \frac{\delta\text{Ro}}{1 - \text{Ro}} - \frac{\delta f}{f}. \quad (11)$$

For example, if  $\text{Ro} = 0.2$ , and if we neglect changes in the relevant value of the Coriolis parameter near the center of the Hadley cells, a 10% increase in the strength of the mean meridional mass flux requires a 10% increase in  $\mathcal{S}$ , or an increase in  $\text{Ro}$  of  $\delta\text{Ro} = 0.08$  or 40%, or a combination of these two kinds of changes. A 40% increase in  $\text{Ro}$  implies the same increase in the rela-

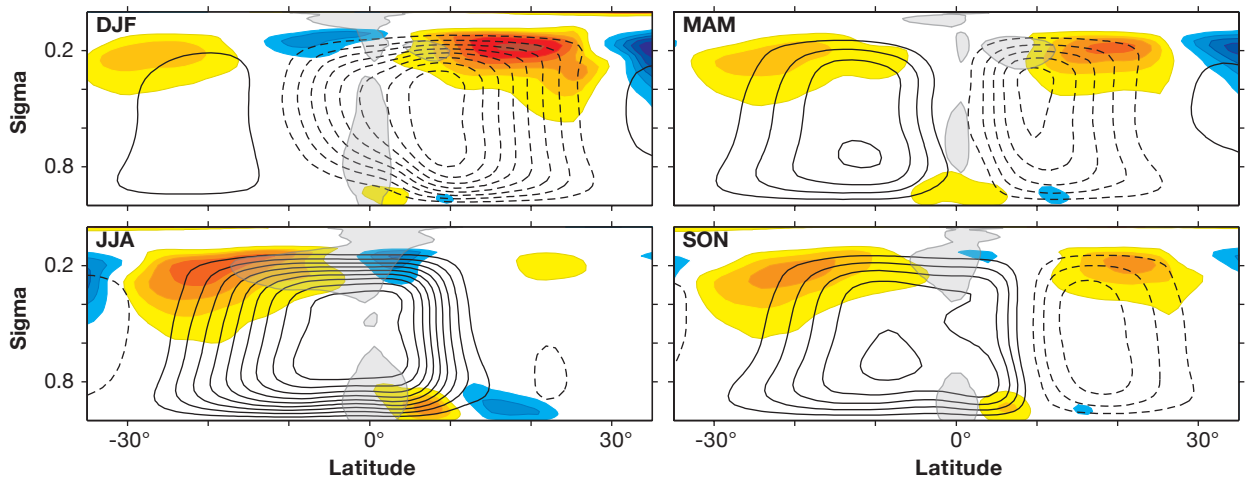


**Figure 5.** Earth’s Hadley circulation over the course of the seasonal cycle. Black contours show the mass flux streamfunction, with dashed (negative) contours indicating clockwise motion and solid (positive) contours indicating counterclockwise motion (contour interval  $25 \times 10^9 \text{ kg s}^{-1}$ ). Colors indicate horizontal eddy momentum flux divergence  $\text{div}(\bar{u}'v' \cos \phi)$ , with the overbar denoting the seasonal and zonal mean and primes denoting deviations therefrom (contour interval  $8 \times 10^{-6} \text{ m s}^{-2}$ , with red tones for positive and blue tones for negative values). Gray shading indicates regions in which  $|\text{Ro}| > 0.5$ . The vertical coordinate  $\sigma = p/p_s$  is pressure  $p$  normalized by surface pressure  $p_s$ . Computed from reanalysis data for the years 1980–2001 provided by the European Centre for Medium-Range Weather Forecasts [Källberg et al., 2004; Uppala et al., 2005].

tive vorticity (meridional shear of the zonal wind) and hence a similarly strong increase in upper-tropospheric zonal winds. Such a strong increase in zonal winds would almost certainly affect the eddy momentum flux divergence  $\mathcal{S}$  substantially. For example, according to the scaling laws in *Schneider and Walker* [2008], the eddy momentum flux divergence scales at least with the square root of meridional surface temperature gradients and thus upper-tropospheric zonal winds (by thermal wind balance). So for small  $Ro$  in general, changes in  $\mathcal{S}$  are strongly implicated in any changes in Hadley circulation strength. Conversely, if  $Ro = 0.8$  under the same assumptions, a 10% increase in the strength of the mean meridional mass flux requires an increase in  $Ro$  of only  $\delta Ro = 0.02$  or 2.5%—implying much subtler changes in upper-tropospheric zonal winds with a weaker effect on eddy momentum fluxes. So for large  $Ro$  in general, changes in  $\mathcal{S}$  play a reduced role in changes in Hadley circulation strength, which therefore can respond more directly to climate changes via changes in energetic and hydrologic balances.

Earth's Hadley cells most of the year exhibit relatively small local Rossby numbers in their upper branches, but local Rossby numbers and the degree to which the Hadley cells are influenced by eddy momentum fluxes vary over the course of the seasonal cycle. Figure 5 shows Earth's Hadley circulation and the horizontal eddy momentum flux divergence for December–January–February (DJF), March–April–May (MAM), June–July–August (JJA), and September–October–November (SON). Also shown are the regions in which  $|Ro| > 0.5$  in the zonal and seasonal mean, that is, regions in which nonlinear momentum advection by the mean meridional circulation is a dominant term in the zonal momentum balance. It is evident that the strength of the DJF, MAM, and SON Hadley cells in both hemispheres is primarily controlled by the eddy momentum flux divergence ( $|Ro| < 0.5$  throughout much of their upper branches above their centers, with  $|Ro| \ll 1$  in the summer and equinox cells); only the strength of the cross-equatorial JJA Hadley cell is not primarily controlled by the eddy momentum flux divergence ( $Ro \gtrsim 0.5$  in much of its upper branch) [*Walker and Schneider* 2005, 2006; *Schneider and Bordoni* 2008; see *Dima et al.* 2005 for a more detailed analysis of the tropical zonal momentum balance]. Nonlinear momentum advection by the mean meridional circulation is a dominant term in the zonal momentum balance in the upper branch of the cross-equatorial JJA Hadley cell, which primarily consists of the Asian summer monsoon circulation [*Dima and Wallace*, 2003]. In the annual mean, Earth's Hadley cells have  $|Ro| < 0.5$  throughout their upper branches, so their strength as well as that of the DJF, MAM, and SON Hadley cells responds to climate changes primarily via changes in the eddy momentum flux divergence. Consistent with these observations, interannual variations in the strength of the DJF Hadley cells are corre-

lated with interannual variations in the eddy momentum flux divergence [*Caballero*, 2007], and differences in strength of the DJF Hadley cells among climate models are correlated with differences in the momentum flux divergence owing to stationary eddies [*Caballero*, 2008]. However, the response of monsoonal circulations to climate changes may be more directly controlled by energetic and hydrologic balances and may differ from the response of the Hadley cells during the rest of the year [*Bordoni and Schneider*, 2008]. And while eddy momentum fluxes constrain the strength of the Hadley cells, that is, the streamfunction extremum at the center of the cells, they do not necessarily constrain where the ascent occurs and thus the position of the Intertropical Convergence Zone, as local Rossby numbers in the ascending branches can be large (Fig. 5).

In the idealized GCM simulations, local Rossby numbers and the degree to which eddy momentum fluxes influence the strength of the Hadley circulation vary with climate. The Hadley circulation is generally more strongly influenced by eddy momentum fluxes in colder climates than in warmer climates: the local Rossby number in the upper branches increases from  $\lesssim 0.5$  in the coldest simulation to  $\lesssim 0.8$  in the warmest simulation (Fig. 6). So understanding how the eddy momentum flux divergence in low latitudes changes with climate is one important part of what needs to be understood to explain how the strength of the Hadley circulation changes in the simulations, but the nonlinear momentum advection by the mean meridional circulation must also be taken into account. However, the Hadley circulation in the simulations is generally less strongly influenced by eddy momentum fluxes than Earth's Hadley cells during equinox or in the annual mean (cf. Fig. 5). This is a consequence of neglecting ocean heat transport, which dominates the meridional heat transport in Earth's low latitudes [*Trenberth and Caron*, 2001]. Neglecting it leads to stronger Hadley cells—e.g., by about 60% in our reference simulation compared with Earth's equinox or annual mean (compare Figs. 5 and 6), or by up to  $O(1)$  factors in simulations with comprehensive GCMs [*Herweijer et al.*, 2005; *Lee et al.*, 2008]. As a result, the nonlinear momentum advection by the mean meridional circulation is stronger and the Hadley cells are closer to the angular momentum-conserving limit than Earth's Hadley cells. Neglecting the coupling of ocean heat transport to the strength of the Hadley circulation [*Klinger and Marotzke*, 2000; *Held*, 2001] thus may lead to different responses of the Hadley circulation to the seasonal cycle or to climate changes, as seen, for example, in the simulations in *Clement* [2006] or *Otto-Bliesner and Clement* [2005]. Therefore, any theory of how the Hadley circulation responds to climate changes must build upon not only a theory of how eddy momentum fluxes change with climate but also a theory of how ocean heat transport is coupled to and modifies the Hadley circulation.

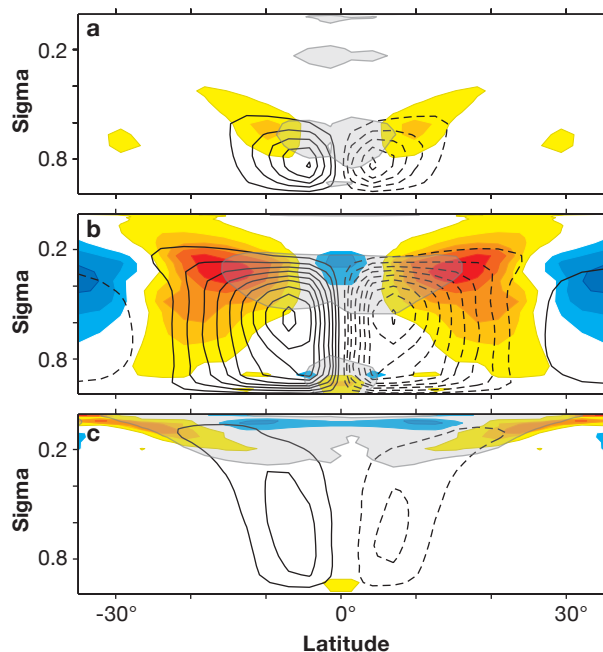


**Figure 6.** Hadley circulations in three idealized GCM simulations. (a) Coldest simulation (global-mean surface temperature  $\langle T_s \rangle = 259$  K). (b) Reference simulation ( $\langle T_s \rangle = 288$  K). (c) Warmest simulation ( $\langle T_s \rangle = 316$  K). Plotting conventions are as in Fig. 5, but with contour interval  $20 \times 10^9 \text{ kg s}^{-1}$  for streamfunction (black) and  $4 \times 10^{-6} \text{ m s}^{-2}$  for horizontal eddy momentum flux divergence (colors). Gray shading again indicates regions in which  $|\text{Ro}| > 0.5$ .

Like the tropical gross upward mass flux, the strength of the Hadley circulation in the idealized GCM simulations changes non-monotonically with global-mean surface temperature. The mass flux in the Hadley cells is  $104 \times 10^9 \text{ kg s}^{-1}$  in the coldest simulation,  $184 \times 10^9 \text{ kg s}^{-1}$  in the reference simulation, and  $51 \times 10^9 \text{ kg s}^{-1}$  in the warmest simulation (Fig. 6). It is maximal in climates slightly colder than that of present-day Earth (see Fig. 4, which shows the vertical mass flux between the equator and  $4^\circ$  at 825 hPa, but this closely approximates the strength of the Hadley cells, or the streamfunction extremum). We have obtained qualitatively similar behavior of the Hadley circulation strength in idealized GCM simulations that do take coupling to ocean heat transport into account [Levine and Schneider, 2009]. This shows that the strength of the Hadley circulation need not always decrease as the climate warms, although it is plausible that it does so as the climate warms relative to that of present-day Earth. Nonetheless, the Hadley circulation may also have been weaker in much colder climates, such as that of the LGM or of a completely ice-covered “snowball” Earth, which may have occurred  $\sim 750$  million years ago [Hoffman et al., 1998]. However, the presence of sea and land ice and ice-albedo feedbacks, which we ignored, may modify the behavior seen in the idealized GCM simulations.

Part of the reason for the non-monotonic change in Hadley circulation strength with global-mean surface temperature is that eddy momentum fluxes influence the Hadley circulation strength and themselves change non-monotonically (see the color contours in Fig. 6). The eddy momentum flux divergence within the Hadley circulation scales similarly to the extratropical eddy kinetic energy [Schneider and Walker, 2008], which changes non-monotonically with global-mean surface temperature (see Fig. 8 below). The reasons for the non-monotonic change in eddy kinetic energy will be discussed further in Section 4.1. However, the changes in eddy momentum flux divergence and eddy kinetic energy do not completely account for the changes in Hadley circulation strength because local Rossby numbers and the degree to which eddy momentum fluxes influence the Hadley circulation vary with climate.

Because the strength of the Hadley circulation is partially controlled by eddy momentum fluxes and extratropical eddy kinetic energies, it bears no obvious relation to the tropical gross upward mass flux, which is more directly controlled by energetic and hydrologic balances. In general, reasoning about the strength of the Hadley circulation that focuses on energetic and hydrologic balances alone and does not take eddy momentum fluxes into account is likely going to be inadequate, given the relatively small local Rossby numbers in Earth’s Hadley cells most of the year.

We currently do not have a theory of how the Hadley circulation strength changes with climate. We have theories for the limit  $\text{Ro} \rightarrow 1$  [Schneider, 1977; Held and Hou, 1980], in which eddy momentum fluxes play no role. We have theories for the limit  $\text{Ro} \rightarrow 0$  [e.g., Dickinson, 1971; Schneider and Lindzen, 1977; Fang and Tung, 1994], in which nonlinear momentum advection by the mean meridional circulation plays no role and one needs primarily a theory of how eddy momentum fluxes change with climate (such as presented in Schneider and Walker [2008] for dry atmospheres). What we need is a theory that can account for interacting changes in the mean meridional circulation and in eddy momentum fluxes, including changes in the relative importance of nonlinear momentum advection by the mean meridional circulation. Shallow-water models of the Hadley circulation in which eddy effects are parameterized may be a starting point for the development of such a theory [Sobel and Schneider, 2009].

Our discussion has focused on the eddy momentum flux as the primary eddy influence on the strength of the Hadley circulation. Eddies can also influence the strength of the Hadley circulation through their energy transport [e.g., Kim and Lee, 2001; Becker and Schmitz, 2001]. For example, the Hadley circulation is constrained by the requirement that diabatic heating in the tropics balance cooling in the subtropics by both radiative processes and eddy energy export to the extratropics. However, unlike the momentum transport, the energy transport by eddies throughout the bulk of

Earth's Hadley cells is smaller (albeit not by much) than the transport by the mean meridional circulation, except in the descending branches [Trenberth and Stepaniak, 2003b].<sup>4</sup> It can be incorporated relatively easily into Hadley circulation theories as an additional thermal driving, provided relations between the eddy energy transport and mean fields such as temperature gradients can be established [e.g., Held and Hou, 1980; Schneider, 1984; Schneider and Walker, 2008].

### 3.3. Height of Hadley Circulation

Another change in the Hadley circulation evident in the idealized GCM simulations is that its height, and with it the height of the tropical tropopause, generally increases as the climate warms (Fig. 6). This can be understood from radiative considerations (e.g., Held [1982]; Thuburn and Craig [2000]; Caballero et al. [2008]; see Schneider [2007] for a review).

A simple quantitative relation indicating how the tropical tropopause height changes with climate can be obtained if (i) the tropospheric temperature lapse rate is taken to be constant, (ii) the atmosphere is idealized as semigray (transparent to solar radiation and gray for longwave radiation), and (iii) the stratosphere is taken to be optically thin and in radiative equilibrium (i.e., the effect of the stratospheric circulation on the tropopause height is neglected). The tropopause height  $H_t$  is then related to the surface temperature  $T_s$ , tropospheric lapse rate  $\gamma$ , and emission height  $H_e$  (at which the atmospheric temperature is equal to the emission temperature) through

$$H_t \approx (1 - c) \frac{T_s}{\gamma} + cH_e, \quad (12)$$

where  $c = 2^{-1/4} \approx 0.84$  [Schneider, 2007]. As the concentration of greenhouse gases (or the optical thickness of the longwave absorber) increases, the emission height  $H_e$  and the tropical surface temperature  $T_s$  generally increase. The tropical lapse rate  $\gamma$  generally decreases because it is close to the moist-adiabatic lapse rate, which decreases with increasing temperature. All three factors—increase in  $T_s$ , decrease in  $\gamma$ , and increase in  $H_e$ —contribute to the increase in tropopause height seen in the idealized GCM simulations.

The relation (12) implies for a typical tropical lapse rate of  $6.5 \text{ K km}^{-1}$  that an increase in tropical surface temperature of  $1 \text{ K}$  leads to an increase in tropopause height of  $25 \text{ m}$  if the emission height stays fixed; any increase in the concentration of greenhouse gases implies an increase in emission height, leading to an additional increase in tropopause height (see Thuburn and Craig [2000] and Schneider [2007] for more precise calculations for more realistic atmospheres). Roughly consistent with these arguments, the tropical tropopause height in recent decades has increased by tens of meters [Seidel et al., 2001], and in simulations of climate

change scenarios, it also increases with tropical surface temperature at a rate of  $\sim 10\text{--}100 \text{ m K}^{-1}$  [Santer et al., 2003a, b; Otto-Bliesner and Clement, 2005].

### 3.4. Width of Hadley Circulation

The Hadley circulation appears to have widened in recent decades [Hu and Fu, 2007; Seidel and Randel, 2007; Seidel et al., 2008; Johanson and Fu, 2009], and it also widens, in the annual mean, as surface temperatures increase in many simulations of climate change scenarios [Lu et al., 2007]. How the width of the Hadley circulation is controlled, however, is unclear.

Following the recognition that eddy fluxes are essential for the general circulation [e.g., Defant, 1921; Jeffreys, 1926] and can be generated by baroclinic instability [Charney, 1947; Eady, 1949], it was generally thought that the meridional extent of the Hadley circulation is limited by baroclinic eddy fluxes. But the work of Schneider [1977] and Held and Hou [1980] (and moist generalizations such as that of Emanuel [1995]) made clear that a Hadley circulation even without eddy fluxes, with upper branches approaching the angular momentum-conserving limit, does not necessarily extend to the poles but can terminate at lower latitudes. The Hadley circulation occupies the latitude band over which its energy transport needs to extend to reduce meridional radiative-equilibrium temperature gradients to values that are consistent with thermal wind balance and with a zonal wind that does not violate the constraint of Hide's theorem that there be no angular momentum maximum in the interior atmosphere (Hide [1969]; Held and Hou [1980]; see Schneider [2006] for a review). Held and Hou [1980] calculated the strength and width of a Hadley circulation under the assumptions that (i) the poleward flow in the upper branches is approximately angular momentum-conserving and (ii) the circulation is energetically closed, so that diabatic heating in ascent regions is balanced by radiative cooling in descent regions. In the small-angle approximation for latitudes and for radiative-equilibrium temperatures that decrease quadratically with latitude away from the equator (a good approximation for Earth in the annual mean), the Hadley circulation according to the Held-Hou theory extends to the latitude

$$\phi_{\text{HH}} \approx \left( \frac{5}{3} \frac{gH_t}{\Omega^2 a^2} \frac{\Delta_h}{T_0} \right)^{1/2}, \quad (13)$$

where  $\Omega$  is the planetary angular velocity,  $\Delta_h$  is the (vertically averaged) pole-equator temperature contrast in radiative equilibrium, and  $T_0$  is a reference temperature. Substituting values representative of Earth ( $\Delta_h/T_0 \approx 80 \text{ K}/295 \text{ K}$  and  $H_t \approx 15 \text{ km}$ ) gives the Hadley circulation terminus  $\phi_{\text{HH}} \approx 32^\circ$  (more precisely,  $\phi_{\text{HH}} = 29^\circ$  if the small-angle approximation is not made). Because this latitude is approximately equal to the actual terminus of the Hadley circulation in Earth's atmosphere (cf. Fig. 5), the Held-Hou result (13) was subsequently often taken as relevant for Earth's

atmosphere. If applicable to Earth's atmosphere, it would imply, for example, that the Hadley circulation widens as the tropopause height or the pole-equator temperature contrast increase.

However, it is questionable how relevant (13) is for the response of Earth's Hadley circulation to climate changes. Because Earth's Hadley circulation generally neither approaches the angular momentum-conserving limit nor is it energetically closed (section 3.2), it may respond differently to climate changes. Indeed, even in simulations with an idealized dry GCM, the width of the Hadley circulation does not behave as indicated by (13) in parameter regimes in which the Rossby number in the circulation's upper branches is similar to that in Earth's atmosphere [Walker and Schneider, 2006]. For example, the Hadley circulation widens much more slowly with increasing radiative-equilibrium pole-equator temperature contrast than indicated by (13); it also widens with increasing low-latitude static stability, whereas (13) would imply it is independent of static stability.

The dependence of the width of the Hadley circulation on the low-latitude static stability suggests a link to baroclinic eddy fluxes. In dry atmospheres, an increased static stability means that the latitude at which baroclinic eddy fluxes first become deep enough to reach the upper troposphere moves poleward [Held, 1978; Schneider and Walker, 2006]. Therefore, it is plausible to attribute the widening of the Hadley circulation with increasing low-latitude static stability to a poleward displacement of deep baroclinic eddy fluxes [Walker and Schneider, 2006; Korty and Schneider, 2008]. Making this notion more precise and harking back to earlier ideas about what terminates the Hadley circulation, one may suppose that the Hadley circulation extends up to the lowest latitude  $\phi_e$  at which meridional eddy entropy fluxes are deep enough to reach the upper troposphere [Korty and Schneider, 2008]. At this latitude, wave activity generated near the surface first reaches the upper troposphere, as the meridional eddy entropy flux is proportional to the vertical wave activity flux [e.g., Edmon et al., 1980]. Because meridional wave activity fluxes in the upper troposphere can be expected to diverge poleward of  $\phi_e$  (where vertical wave activity fluxes converge) and because the meridional wave activity flux divergence is proportional to the eddy momentum flux convergence, there is upper-tropospheric eddy momentum flux convergence poleward of  $\phi_e$  and divergence equatorward of  $\phi_e$  [e.g., Held, 1975, 2000; Simmons and Hoskins, 1978; Edmon et al., 1980]. At the latitude  $\phi_e$ , then, the eddy momentum flux divergence  $\mathcal{S}$  in the upper troposphere changes sign. Because the local Rossby number is generally small near the subtropical termini of the Hadley circulation, the zonal momentum balance (10) there is approximately

$$f\bar{v} \approx \mathcal{S}, \quad (14)$$

so that a change in sign in  $\mathcal{S}$  implies a change in sign in the meridional mass flux: the latitude  $\phi_e$  marks the transition between the Hadley cells, near whose subtropical termini  $\mathcal{S} > 0$  and  $\bar{v}$  is poleward, and the Ferrel cells, in which  $\mathcal{S} < 0$  and  $\bar{v}$  is equatorward (Figs. 5 and 6).

With this notion of what terminates the Hadley circulation, it remains to relate the height reached by substantial eddy entropy fluxes to the mean temperature structure and other mean fields and parameters. In dry atmospheres, the supercriticality

$$S_c = -\frac{f}{\beta} \frac{\partial_y \bar{\theta}_s}{\Delta_v} \sim \frac{\bar{p}_s - \bar{p}_e}{\bar{p}_s - \bar{p}_t}, \quad (15)$$

is a nondimensional measure of the pressure range over which eddy entropy fluxes extend (Schneider and Walker [2006]; Schneider [2007]; see Held [1978] for a similar measure in quasigeostrophic theory). Here,  $\beta = 2\Omega a^{-1} \cos \phi$  is the meridional derivative of the Coriolis parameter  $f$ ;  $\bar{\theta}_s$  is the mean surface or near-surface potential temperature;  $\Delta_v$  is a bulk stability measure that depends on the near-surface static stability; and  $\bar{p}_s$ ,  $\bar{p}_t$ , and  $\bar{p}_e$  are the mean pressures at the surface, at the tropopause, and at the level up to which eddy entropy fluxes extend. Consistent with the preceding discussion, the Hadley circulation in dry GCM simulations, in parameter regimes comparable with Earth's, extends up to the latitude  $\phi_e$  at which the supercriticality (15), evaluated locally in latitude, first exceeds a critical  $O(1)$  value [Korty and Schneider, 2008]. In particular, the Hadley circulation generally widens as the bulk stability  $\Delta_v$  increases, consistent with the increase in  $\Delta_v$  at the subtropical termini being primarily compensated by an increase in  $f/\beta = a \tan \phi_e$ .

There are two challenges to obtain a closed theory of the width of the Hadley circulation from these results. First, for dry atmospheres, the mean fields in the supercriticality (15) need to be related to the mean meridional circulation and eddy fluxes, which determine them in concert with radiative processes. For a Hadley circulation whose upper branches approach the angular momentum-conserving limit, an expression for the width can be derived in which the meridional surface potential temperature gradient no longer appears explicitly [Held, 2000]; however, because the Hadley circulation generally does not approach the angular momentum-conserving limit, the resulting expression does not accurately account for changes in the width, even in dry GCM simulations [Walker and Schneider, 2006; Schneider, 2006; Korty and Schneider, 2008]. (Some recent papers have advocated similar expressions to account for the relatively modest changes in the Hadley circulation width seen in simulations of climate change scenarios [e.g., Lu et al., 2007; Frierson et al., 2007b], but the results from the much broader range of dry GCM simulations in Walker and Schneider [2006] and Korty and Schneider [2008] show that these expressions cannot be generally adequate.) In addition to



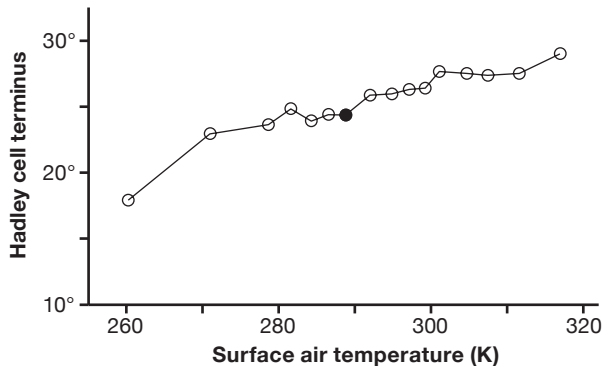


**Figure 7.** Hadley circulation width vs global-mean surface temperature in idealized GCM simulations. Shown is the latitude of the subtropical terminus of the Hadley circulation, defined as the latitude at which the mass flux streamfunction at approximately 725 hPa is zero. The termination latitudes in both hemispheres are averaged.

the meridional surface potential temperature gradient, one needs to close for the near-surface static stability, which likewise depends on the flow. The static stability at the subtropical termini of the Hadley circulation cannot simply be viewed as controlled by convection, as in the deep tropics, but it is influenced by the mean meridional circulation and eddy fluxes.

Second, for moist atmospheres, the supercriticality (15) does not generally give a good estimate of the height reached by substantial eddy entropy fluxes [Schneider and O’Gorman, 2008]. The difficulties in relating the static stability at the subtropical termini of the Hadley circulation to mean flows and eddy fluxes are exacerbated in moist atmospheres, in which it is unclear what the effective static stability is that eddy fluxes experience, how that effective static stability is controlled, and how it relates to the depth of eddy entropy fluxes. We currently do not have theories of the static stability and Hadley circulation width that are adequate for moist atmospheres.<sup>5</sup>

In the idealized GCM simulations presented throughout this paper, the width of the Hadley circulation increases modestly with surface temperature. The Hadley circulation extends to 18° latitude in the coldest simulation, to 24° in the reference simulation, and to 29° latitude in the warmest simulation. The Hadley circulation in the reference simulation is narrower than Earth’s—at least in part because ocean heat transport is neglected, so that meridional surface temperature gradients in the tropics are larger than on Earth. The increase in the width of the Hadley circulation with surface temperature is qualitatively consistent with the notion that baroclinic eddy fluxes terminate the Hadley circulation, and that the latitude at which they reach the upper troposphere moves poleward as the subtropical static stability increases, in part but not exclusively because the moist-adiabatic lapse rate decreases with temperature. However, the increase in the width is not quantitatively

consistent with the arguments for dry atmospheres. Devising a theory that accounts for these results remains as one of the fundamental challenges in completing a theory of the general circulation of moist atmospheres.

#### 4. EXTRATROPICAL CIRCULATIONS

One measure of the importance of water vapor and latent heat release in extratropical circulations is the fraction of the poleward energy flux that takes the form of a latent heat flux. In the present climate, this is about half of the total atmospheric energy flux in midlatitudes [Pierrehumbert, 2002; Trenberth and Stepaniak, 2003b], indicating a significant role for water vapor in extratropical dynamics. But whereas water vapor plays an unambiguously important role in tropical dynamics, its role in extratropical dynamics is less clear.

Moist convection in the extratropics is not as ubiquitous as it is in the tropics (over oceans, it primarily occurs in fronts of large-scale eddies), so that the precise dynamical role of water vapor in the extratropics is unclear. The importance of water vapor in extratropical dynamics may depend strongly on the warmth of the climate considered, as surface temperatures in the extratropics respond more strongly to climate changes than in the tropics, and the saturation vapor pressure and thus the near-surface specific humidity depend nonlinearly on temperature. Water vapor likely has a much reduced dynamical role in the extratropics of cold climates, such as that of the LGM, and a correspondingly greater role in hothouse climates. The unclear role of water vapor in extratropical dynamics in the present climate and its changed importance in colder or warmer climates are principal challenges in understanding extratropical circulations and their response to climate changes.

##### 4.1. Transient eddy kinetic energy

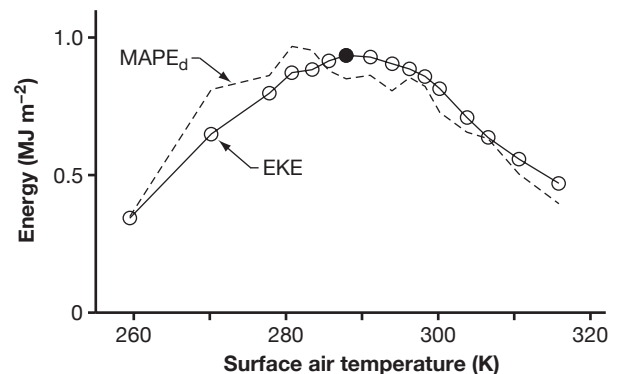


**Figure 8.** Total eddy kinetic energy (EKE) (solid line with circles), and rescaled dry mean available potential energy (MAPE<sub>d</sub>) (dashed line) vs global-mean surface temperature in idealized GCM simulations. Averages are taken over baroclinic zones in both hemispheres. MAPE<sub>d</sub> is evaluated for the troposphere and is rescaled by a constant factor of 2.4. (Adapted from O’Gorman and Schneider [2008b].)

Several lines of evidence point to an influence of latent heat release on the structure and amplitude of extratropical storms, ranging from studies of individual cyclones [e.g., *Reed et al.*, 1988; *Wernli et al.*, 2002], to theoretical considerations of the effect of water vapor on the mean available potential energy [*Lorenz*, 1978]. The mean available potential energy is a measure of the energy available to midlatitude transient eddies through adiabatic air mass rearrangements [*Peixoto and Oort*, 1992, chapter 14]. It is always greater when the potential release of latent heat in condensation of water vapor is taken into account. For a zonal-mean state similar to that of the present climate, the mean moist available potential energy is roughly 30% greater than the mean dry available potential energy [*Lorenz*, 1979]. Latent heat release also increases the linear growth rate of moist baroclinic eddies [*Bannon*, 1986; *Emanuel et al.*, 1987], leads to greater peak kinetic energy in lifecycle studies of baroclinic eddies [*Gutowski et al.*, 1992], and contributes positively to the budget of eddy available potential energy in Earth's storm tracks [*Chang et al.*, 2002].

It is therefore somewhat surprising that the total (vertically integrated) eddy kinetic energy scales approximately linearly with the dry mean available potential energy in the idealized GCM simulations (Fig. 8). The energies shown are averaged meridionally over baroclinic zones, which are here taken to be centered on maxima of the eddy potential temperature flux and to have constant width  $L_Z$  corresponding to  $30^\circ$  latitude [*O'Gorman and Schneider*, 2008b]. Both the eddy kinetic energy and the dry mean available potential energy have a maximum for a climate close to that of present-day Earth and are smaller in much warmer and much colder climates (Fig. 8). Similar behavior is found for the near-surface eddy kinetic energy: surface storminess likewise is maximal in a climate close to that of present-day Earth (Fig. 9). Broadly consistent with the idealized GCM simulations, simulations with comprehensive GCMs suggest that extratropical storms change only modestly in strength when the present climate changes [*Geng and Sugi*, 2003; *Yin*, 2005; *Bengtsson et al.*, 2006, 2009], and they can be weaker both in glacial climates [*Li and Battisti*, 2008] and in warm, equable climates [e.g., *Rind*, 1986; *Korty and Emanuel*, 2007].

To understand why the energies in the idealized GCM are maximal in a certain climate, it is useful to consider the approximate dry mean available potential energy

$$\text{MAPE}_d \approx \frac{c_p}{24g} \Delta p_t L_Z^2 \Gamma (\partial_y \bar{\theta})^2, \quad (16)$$

obtained as a scaling approximation of Lorenz's [1955] mean available potential energy [*Schneider*, 1981; *Schneider and Walker*, 2008; *O'Gorman and Schneider*, 2008b]. Here,  $\Delta p_t = \bar{p}_s - \bar{p}_t$  is the pressure depth

of the troposphere,

$$\Gamma = -\frac{\kappa}{p} (\partial_p \bar{\theta})^{-1} \quad (17)$$

is an inverse measure of the dry static stability,  $\partial_y \bar{\theta}$  is the mean meridional potential temperature gradient,  $\kappa$  is the adiabatic exponent, and  $g$  is the gravitational acceleration. The meridional potential temperature gradient and inverse static stability are understood to be averaged vertically over the depth of the troposphere and meridionally over baroclinic zones, in addition to zonally and temporally [*O'Gorman and Schneider*, 2008b]. According to the approximation (16),  $\text{MAPE}_d$  increases with increasing meridional potential temperature gradients and tropopause height and with decreasing static stability. In the idealized GCM simulations, several factors conspire to lead to the non-monotonic behavior of  $\text{MAPE}_d$ :

(i) As the climate warms relative to the reference climate, the vertically averaged meridional potential temperature gradient decreases and the static stability increases (see Fig. 11 below). These changes in the thermal structure of the troposphere primarily result from increased poleward and upward transport of latent heat.

There is also a countervailing increase in tropopause height (it changes for the reasons discussed in section 3.3), but the combined changes in static stability and temperature gradient are larger and result in a decrease in  $\text{MAPE}_d$ .

(ii) As the climate cools relative to the reference climate, the near-surface meridional potential temperature gradient increases strongly. The vertically averaged meridional potential temperature gradient also increases, albeit less strongly than the near-surface gradient because the tropical temperature lapse rate, which is approximately moist adiabatic, increases, whereas the extratropical lapse rate, which is at least partially determined by baroclinic eddies (see section 4.4 below), decreases. In  $\text{MAPE}_d$ , the increase in the vertically averaged meridional potential temperature gradient is overcompensated by decreases in the tropopause height and by the increase in the extratropical static stability.

It is noteworthy that changes in the eddy kinetic energy need not be of the same sign as changes in the near-surface meridional temperature gradient, contrary to what is sometimes assumed in discussions of extratropical storminess (e.g., at the LGM). In the idealized GCM simulations, the near-surface meridional temperature gradient decreases monotonically as the climate warms, whereas the eddy kinetic energy (and  $\text{MAPE}_d$ ) change non-monotonically.

The scaling of the eddy kinetic energy with the dry mean available potential energy intimates that water vapor dynamics affects the eddy kinetic energy in the idealized GCM primarily through its effect on the thermal structure of the troposphere, rather than through direct effects of latent heat release on eddies. Be-

cause extratropical water vapor dynamics generally decreases meridional potential temperature gradients and increases the (dry) static stability, it primarily damps eddies, rather than energizing them, as one might have inferred from the fact that in Earth's storm tracks, latent heat release contributes positively to the budget of eddy available potential energy [cf. *Chang et al.*, 2002]. Although it may seem surprising and is largely an empirical result that the eddy kinetic energy scales with the dry mean available potential energy and thus depends on the dry static stability, there are several plausible reasons for this [*O'Gorman and Schneider*, 2008b]. For example, the 30% difference between mean dry and moist available potential energies that *Lorenz* [1979] found for the present climate largely arises owing to water vapor in tropical low-level regions, which may not be important for midlatitude eddies. Additionally, changes in the effective moist static stability that midlatitude eddies experience may generally scale with changes in the dry static stability if the effective moist static stability is a weighted average of a dry stability and a smaller moist stability in updrafts [*Emanuel et al.*, 1987], and if the weighting coefficients (e.g., the area fractions of updrafts and downdrafts) do not change substantially with climate.

Does the eddy kinetic energy always scale with the dry mean available potential energy, as in the idealized GCM, or can latent heat release directly energize the statistically steady state of baroclinic eddies? *Lapeyre and Held* [2004] analyzed the moist eddy available potential energy budget of a two-layer quasigeostrophic model with water vapor in the lower layer. In the model, increases in the production of moist eddy available potential energy associated with latent heat release are primarily balanced by water vapor diffusion and dehumidification processes, rather than by conversion to eddy kinetic energy, implying an inefficient heat engine. For very strong latent heat release, a vortex-dominated regime emerged that had no analog in a corresponding dry model. While the study of *Lapeyre and Held* [2004] provides some guidance to the possible role of water vapor in the dynamics of baroclinic eddies in a statistically steady state, it is difficult to relate these results to the behavior of moist baroclinic eddies in general circulation models or in the real atmosphere.

We have used averages of the eddy kinetic energy to give a general description of the effect of water vapor on the amplitude of baroclinic eddies. However, this does not tell us about the possible effects of changes in latent heat release, for example, on mesoscale wind extremes or on the local energy of cyclones in zonally confined storm tracks. Changes in the structure of baroclinic eddies due to latent heat release also affect the magnitude and extent of updrafts [*Emanuel et al.*, 1987; *Zurita-Gotor*, 2005], which can be expected to influence extratropical precipitation and its extremes. Extratropical mean precipitation and precipitation ex-

trêmes generally increase in intensity as the climate warms, albeit at a smaller rate than the mean specific humidity [*O'Gorman and Schneider*, 2009a, b].

## 4.2. Position of storm tracks

The extratropical storm tracks generally shift poleward as the climate warms in simulations of climate change scenarios [*Yin*, 2005; *Bengtsson et al.*, 2006]. They also shift poleward as the climate warms in the idealized GCM simulations [*O'Gorman and Schneider*, 2008a], provided storm tracks are identified with regions of large near-surface eddy kinetic energy (Fig. 9).<sup>6</sup>

Attempts have been made to relate changes in the position of extratropical storm tracks to changes in local measures of baroclinic instability. The Eady growth rate is typically used as the measure of baroclinic instability [e.g., *Lindzen and Farrell*, 1980; *Hoskins and Valdes*, 1990; *Geng and Sugi*, 2003; *Yin*, 2005; *Li and Battisti*, 2008; *Brayshaw et al.*, 2008]. It depends on the meridional potential temperature gradient and the dry static stability and is similar to the square root of the mean available potential energy (16). *Yin* [2005] found that changes in the Eady growth rate in climate change simulations seemed to account for a poleward shift in the eddy kinetic energy maximum, and that more of the change was related to the meridional potential temperature gradient than to the static stability. However, it is not clear how the local linear growth rate of baroclinic instability relates to the distribution of eddy kinetic energy in a statistically steady state. For example, the Eady growth rate in the idealized GCM simulations typically has two maxima as a function of latitude, one near the subtropical terminus of the Hadley cell, and one in midlatitudes. In warm simulations, the subtropical maximum in growth rate is the hemispheric maximum, but it is located equatorward of the storm track.

Latent heat release helps to set the mean thermal structure of the troposphere and thus indirectly affects

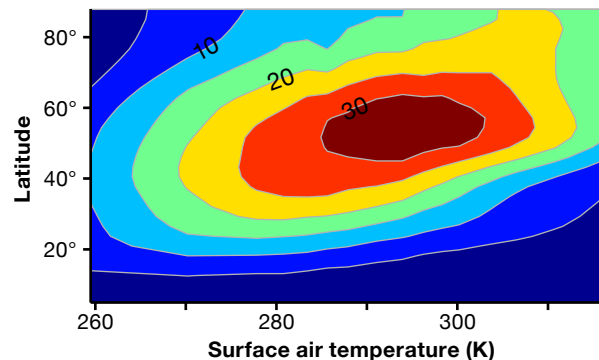


**Figure 9.** Near-surface eddy kinetic energy (contour interval  $5 \text{ kJ m}^{-2}$ ) as a function of global-mean surface temperature and latitude in idealized GCM simulations. The near-surface eddy kinetic energy is integrated from the surface to  $\sigma = 0.9$ .

the dry Eady growth rate and other measures of baroclinicity. But it can also directly affect the growth rate of baroclinic instability, an effect which probably must be taken into account when considering climate changes, given how rapidly precipitable water increases with temperature. *Orlanski* [1998] proposed using an approximate result for the moist baroclinic instability growth rate based on the work of *Emanuel et al.* [1987] but he found that the inclusion of latent heat release only modestly affects the growth rates in the winter storm track. It remains unclear how growth rates of baroclinic instability depend on the mean state of a moist atmosphere, and how they relate to storm track position in other seasons or in very warm climates.

*Chen and Held* [2007] proposed a different approach to understanding shifts in the storm tracks, based on considering changes in the momentum fluxes associated with upper-tropospheric eddies. Key to the mechanism they propose are changes in upper-tropospheric and lower-stratospheric zonal winds that are linked, by thermal wind balance, to changes in the thermal structure near the tropopause. For example, increases in the concentration of greenhouse gases generally lead to lower-stratospheric cooling and upper-tropospheric warming, which imply a strengthening of lower-stratospheric zonal (westerly) winds around the poleward and downward sloping extratropical tropopause. Such changes can modulate the phase speed of upper-tropospheric eddies and may, via a shift in their critical latitude, lead to a shift in the position of storm tracks. Unlike the other mechanisms we discussed, this mechanism relies on radiative changes in the lower stratosphere, which are not well represented by the simplified radiation scheme of our idealized GCM. Since the dynamics of upper-tropospheric eddies are largely unaffected by latent heat release, the mechanism also does not allow for a direct role for water vapor dynamics.

There currently is no comprehensive theory for the position of storm tracks, even in the zonal mean. It is

even less clear what determines the longitudinal extent of zonally varying storm tracks [*Chang et al.*, 2002].

### 4.3. Poleward energy flux

The poleward energy flux in the extratropics, effected primarily by eddies, is essential to the maintenance of climate, particularly in high latitudes. The total energy flux can be divided into the atmospheric fluxes of dry static energy,  $c_p T + gz$ , and latent heat,  $Lq$ , plus the ocean heat flux; the kinetic energy flux is negligible in both the atmosphere and oceans [*Peixoto and Oort*, 1992]. In the idealized GCM simulations, the relative contributions to the extratropical poleward energy flux from dry static energy and latent heat vary strongly with climate (Fig. 10). The dry static energy flux dominates in cold climates; the latent heat flux dominates in warm climates. The total poleward energy flux does not remain constant as the climate varies, but it increases from the coldest to moderately warm simulations and decreases again in the warmest simulations. Close to the reference simulation, there is some compensation between opposing changes in latent heat and dry static energy fluxes, but the compensation is not exact and not a general feature of climate changes: in cold simulations, for example, changes in latent heat and dry static energy fluxes have the same sign. This stands in contrast to the almost exact compensation between changes in poleward energy flux components that *Frierson et al.* [2007a] found in a similar idealized GCM as they varied the amount of water vapor in the atmosphere, keeping radiative transfer parameters fixed. The difference in behavior most likely results from the difference in how the climate is varied (changing longwave optical thickness vs changing water vapor concentrations while keeping radiative parameters fixed). Figure 10 shows that a compensation between changes in poleward energy flux components cannot generally be expected in response to climate changes such as those induced by changes in greenhouse gas concentrations.

How the poleward energy flux changes with climate is relevant to several fundamental questions, including the question of how small the pole-equator temperature contrast can get in equable climates, given the insolation distribution. For very warm climates, it becomes essential to understand the scaling of the poleward latent heat flux because it dominates the total poleward energy flux in such climates. In the extratropics, the poleward latent heat flux is dominated by the eddy component  $\mathcal{F}_e = \{Lv'q'\}$ , which scales like

$$\mathcal{F}_e \sim Lv_e q_{\text{ref}} p_0 / g, \quad (18)$$

where  $q_{\text{ref}}$  is a subtropical reference specific humidity,  $v_e$  is an eddy velocity scale, and  $p_0$  is the mean surface pressure [*Pierrehumbert*, 2002; *Caballero and Langen*, 2005; *O’Gorman and Schneider*, 2008a]. The scaling derives from the assumption that the eddy flux of latent heat is effected by eddies that pick up water vapor in or near the boundary layer in the subtropics and transport

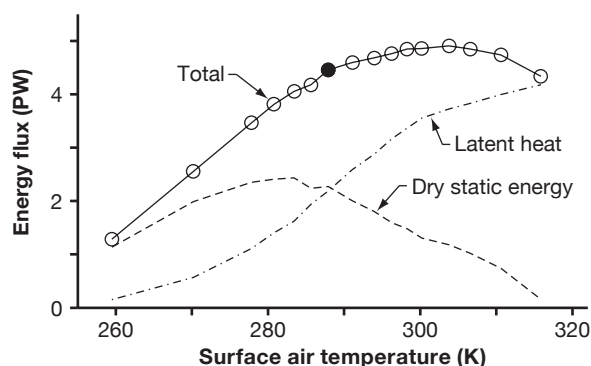


**Figure 10.** Vertically integrated poleward energy flux (solid line and circles) at 50° latitude vs global-mean surface temperature and decomposition into dry static energy flux (dashed line) and latent heat flux (dash-dotted line). (Adapted from *O’Gorman and Schneider* [2008a].)



it poleward and upward along approximately isentropic paths, along which air masses cool, the specific humidity reaches saturation, and the water vapor condenses out. According to the scaling (18), the decrease in eddy kinetic energy (and thus in  $v_e$ ) in warm climates (Fig. 8) plays a critical role in limiting the poleward latent heat flux and hence the minimum attainable pole-equator temperature contrast [Caballero and Langen, 2005]. Since the eddy kinetic energy itself depends on the pole-equator temperature contrast and on the static stability (as discussed in section 4.1), and since these in turn depend on water vapor dynamics, interesting dynamical feedbacks in which water vapor plays a major role are conceivable. The scaling (18) generally accounts well for the eddy latent heat flux in the idealized GCM simulations, except in the warmest simulations, in which it overestimates the latent heat flux [O’Gorman and Schneider, 2008a]. More sophisticated scalings may be needed for the poleward latent heat flux in very warm climates or at high latitudes; analyses of how water vapor is transported along isentropes and condenses may be useful in this regard [Pierrehumbert et al., 2007; O’Gorman and Schneider, 2006].

The poleward dry static energy flux in the idealized GCM simulations changes non-monotonically with global-mean surface temperature (Fig. 10). As for the eddy kinetic energy, changes in the dry static energy flux can have the opposite sign of changes in the near-surface meridional temperature gradient, contrary to what is sometimes assumed. In the idealized GCM simulations, the dry static energy flux is maximal in climates slightly colder than that of present-day Earth, as is the eddy kinetic energy and the dry mean available potential energy (cf. Fig. 8). Indeed, in dry atmospheres in which baroclinic eddies modify the thermal stratification, the eddy flux of dry static energy, which dominates the extratropical dry static energy flux, scales with  $\text{MAPE}_d/\Gamma^{1/2}$ , that is, with the mean available po-

tential energy modulated by a weak dependence on the static stability  $\Gamma^{-1}$  [Schneider and Walker, 2008]. This scaling derives from assuming that the eddy kinetic energy scales with  $\text{MAPE}_d$ , that eddy kinetic energy and eddy available potential energy are equipartitioned, and that the eddy flux of dry static energy can be related to the eddy kinetic energy and eddy available potential energy. These assumptions are sufficiently well satisfied in the idealized GCM simulations that the scaling correctly suggests a climatic maximum in the dry static energy flux.

#### 4.4. Thermal stratification

The mean thermal stratification of the extratropical troposphere influences important climatic features such as the eddy kinetic energy, the position of storm tracks, and the poleward energy flux. Water vapor dynamics affects the thermal stratification through latent heat release in moist convection and in large-scale condensation. In the idealized GCM simulations, the extratropical static stability increases as the climate warms relative to the reference climate, largely because the poleward and upward transport of latent heat strengthens as the climate warms. However, the extratropical static stability also increases as the climate cools relative to the reference climate (Fig. 11).

In colder climates, the amount of water vapor in the extratropical atmosphere is small, and a dry theory for the thermal stratification accounts for the simulation results: The static stability is proportional to the meridional surface temperature gradient multiplied by  $f/\beta$  evaluated at the storm track latitude, such that the supercriticality (15) averaged over the extratropics satisfies  $S_c \sim 1$  [Schneider and Walker, 2006; Schneider and O’Gorman, 2008]. The static stability thus decreases as the meridional surface temperature gradient decreases and the climate warms ( $f/\beta$  at the storm track latitude increases slightly as the storm tracks shift poleward, but this is overcompensated by the surface temperature gradient decrease). However, latent heat release plays an increasingly important role in the maintenance of the extratropical stratification as the climate warms, primarily through large-scale latent heat fluxes. In warmer climates, the dry theory with  $S_c \sim 1$  is no longer applicable. Static stabilities are generally greater in these warm and moist climates than the dry theory would predict [Schneider and O’Gorman, 2008].

In addition to large-scale latent heat fluxes, moist convection becomes more prevalent in the extratropics in warmer climates. A theory that posits a central role for baroclinic eddies and moist convection has been proposed for the extratropical thermal stratification [Jukes, 2000; Frierson et al., 2006; Frierson, 2008]. However, a direct role for extratropical moist convection in setting the thermal stratification in the idealized GCM simulations is ruled out by a set of simulations in which the temperature lapse rate toward which the convection scheme relaxes tempera-

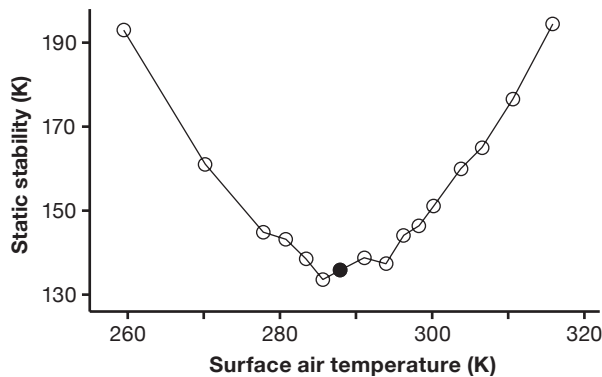


**Figure 11.** Extratropical dry static stability vs global-mean surface temperature in idealized GCM simulations. The static stability is computed by averaging  $\Gamma^{-1}$  (Eq. 17) vertically over the troposphere and meridionally over baroclinic zones in both hemispheres. (Adapted from O’Gorman and Schneider [2008b].)



ture profiles was artificially rescaled to be lower (more stable) than the moist-adiabatic lapse rate; instead of moist convection, large-scale latent heat fluxes appear to be crucial for the extratropical thermal stratification [Schneider and O’Gorman, 2008]. Nonetheless, these results from idealized aquaplanet simulations do not preclude an important role for extratropical (possibly slantwise) moist convection in setting the thermal stratification seasonally or regionally in Earth’s atmosphere [Emanuel, 1988]. For example, moist convection does appear to control the extratropical thermal stratification over some land surfaces in summer [Korty and Schneider, 2007]. The formulation of a general theory of the extratropical thermal stratification that accounts for latent heat release, in moist convection and in large-scale fluxes, remains an outstanding challenge.

Through its effect on the thermal structure of the troposphere and the poleward energy flux, together with indirect (and possibly direct) effects on the extratropical storm tracks, water vapor dynamics play an important role in extratropical circulations, except in very cold climates. To make further progress understanding how extratropical atmospheric dynamics change with climate, it will be necessary to develop theories for extratropical dynamics that take direct account of latent heat release. Such theories must be reducible to existing theories for dry dynamics, but it is unclear to what extent they can be developed through generalization of concepts from dry dynamics (e.g., replacing dry static stabilities by effective moist static stabilities).

## 5. SUMMARY AND OPEN QUESTIONS

We have presented an overview of dynamic effects of water vapor in the global circulation of the atmosphere and in climate changes, illustrated by simulations of a broad range of climates with an idealized GCM. With a review of global energetic constraints on hydrologic variables as point of departure, we discussed how water vapor dynamics affects the tropical gross upward mass flux, how the Hadley circulation changes with climate, and how aspects of extratropical circulations, such as extratropical storminess and the poleward energy transport, relate to and influence the mean climate state. Central conclusions were:

1. Changes in global-mean evaporation and precipitation and in near-surface relative humidity are strongly energetically constrained. Near the present climate, global-mean evaporation and precipitation can increase with surface temperature at a rate of  $O(2\% K^{-1})$ , and the near-surface relative humidity can change by  $O(1\% K^{-1})$ .

2. Because changes in near-surface relative humidity are small and most water vapor is concentrated near the surface, precipitable water increases with surface temperature approximately at the Clausius-Clapeyron rate at which saturation specific humidity increases. Near the present climate, this rate is  $6\text{--}7\% K^{-1}$ .

3. Although the water vapor cycling rate generally decreases as the climate warms, except in very cold climates, the tropical gross upward mass flux does not necessarily decrease at a similar rate, or at all. Rather, the tropical gross upward mass flux may depend on precipitation and the moist-adiabatic static stability of the tropical atmosphere, which changes more slowly with temperature than precipitable water.

4. The Hadley circulation generally widens and increases in height as the climate warms. Changes in its strength are more complex. They are constrained by the zonal momentum balance and the strength of eddy momentum fluxes. Near the present climate, the Hadley cell likely weakens as the climate warms; however, it may also weaken as the climate cools, in part because the eddy momentum fluxes, whose strength is related to the extratropical eddy kinetic energy, can change non-monotonically with climate.

5. The extratropical transient eddy kinetic energy, a measure of storminess, scales with the dry mean available potential energy. Near the present climate, both energies decrease as the climate warms, because meridional potential temperature gradients decrease and the static stability increases as the poleward and upward transport of latent heat strengthens. In colder climates, however, both energies can also decrease as the climate cools.

6. Storm tracks generally shift poleward as the climate warms.

7. The poleward latent heat flux in the extratropics generally increases as the climate warms, but the dry static energy flux can change non-monotonically. The total poleward energy flux, the sum of the two, can also change non-monotonically, suggesting there may exist a limit on how small pole-equator temperature contrasts can become in equable climates.

8. The behavior of the extratropical static stability is complex. Strengthening poleward and upward latent heat transport in warmer and moister climates can increase the static stability. And strengthening meridional surface temperature gradients in colder and drier climates can also lead to an increase in static stability.

A recurring theme was that although hydrologic variables such as global-mean precipitable water and precipitation change monotonically with surface temperature, dynamical variables such as the tropical gross upward mass flux or the extratropical eddy kinetic energy need not change monotonically; they can be weaker than they presently are both in much warmer and in much colder climates.

A number of questions have remained open, chief among them:

1. How do changes in the mean meridional circulation and in eddy momentum fluxes interact to control how the strength of the Hadley circulation changes with climate?

2. How does the width of the Hadley circulation depend on mean fields such as meridional temperature

gradients, the specific humidity, and the (subtropical) static stability?

3. Can latent heat release directly energize the statistically steady state of extratropical eddies? Or is its main effect through modifications of the mean state of the atmosphere?

4. What controls the position of storm tracks and their poleward shift as the climate warms? More generally, how do eddy kinetic energies and other eddy fields depend on mean fields, and what controls their variations with latitude?

5. What controls the static stability of the subtropical and extratropical atmosphere?

The lack of a theory for the subtropical and extratropical static stability runs through several of the open questions. Devising a theory that is general enough to be applicable to relatively dry and moist atmospheres remains as one of the central challenges in understanding the global circulation of the atmosphere and climate changes.

**ACKNOWLEDGMENTS.** We are grateful for support by the Davidow Discovery Fund, the National Science Foundation (Grant ATM-0450059), and a David and Lucile Packard Fellowship. The simulations shown were performed on Caltech's Division of Geological and Planetary Sciences Dell cluster. Portions of section 2 appeared previously in the Proceedings of the 15th 'Aha Huli' Hawaiian Winter Workshop [Schneider and O'Gorman, 2007]. We thank Ian Eisenman, Yohai Kaspi, Tim Merlis, Steven Sherwood, and two reviewers for helpful comments on a draft of this paper.

## NOTES

1. The parameterized convection in the idealized GCM does not contain an explicit representation of subgrid convective mass fluxes. It acts by imposing temperature and specific humidity tendencies, as in the Betts-Miller convection scheme [Betts, 1986; Betts and Miller, 1986, 1993]. Vertical motion on the grid scale is induced by the thermodynamic effects of the parameterized convection, so it consists of convective and (particularly in the extratropics) large-scale components.
2. More precisely, Fig. 4 shows  $\Psi^1$  and  $\Psi$  defined analogously to (9) but in  $\sigma$  coordinates and evaluated at  $\sigma = 0.825$ , where  $\sigma = p/p_s$  (pressure  $p$  over surface pressure  $p_s$ ) is the GCM's vertical coordinate. In what follows, all quantities calculated from GCM simulations and reanalyses are evaluated in  $\sigma$  coordinates, with the appropriate surface pressure-weighting of averages [e.g., Walker and Schneider, 2006]; however, we give approximate pressure levels and expressions in pressure coordinates to simplify the presentation.

3. Held and Soden [2006] and Vecchi and Soden [2007] consider the mid-tropospheric mass flux at 500 hPa, rather than a lower-tropospheric mass flux. Generally they find that the mid-tropospheric gross upward mass flux on the grid scale of the models decreases more slowly than the water vapor cycling rate as the climate warms. In one model, however, the mid-tropospheric convective mass flux scales with the water vapor cycling rate at least over the earlier part of a 21st-century climate change simulation (it varies more slowly in later parts of the simulation). But this latter result may not be general. In our idealized GCM simulations, the mid-tropospheric gross upward mass flux also scales with the water vapor cycling rate near the reference simulation and in warmer simulations, but not in colder simulations (excluding the coldest simulation, in which the tropopause is near or below the 500-hPa level). The mid-tropospheric gross upward mass flux is up to a factor  $\sim 2$  smaller than the lower-tropospheric gross upward mass flux we consider, so the latter may be more clearly related to column-averaged condensation and precipitation, at least in our GCM.
4. Trenberth and Stepaniak [2003a] argue that the "seamlessness" of the energy transport between the tropics and the extratropics provides a constraint on the energy transport and strength of Hadley cells. However, this "seamlessness" of the energy transport is not a fundamental property of atmospheric circulations. We have obtained simulations with idealized GCMs in which the tropical energy transport, dominated by the mean meridional circulation, differs substantially from the extratropical energy transport, dominated by eddies. (For example, this is the case in the simulations in Walker and Schneider [2006] in which the planetary rotation rate is varied.)
5. In addition to the mechanisms sketched here, the width of the Hadley circulation may also change in response to changes in upper-tropospheric wave dynamics that may be caused by lower-stratospheric changes associated with ozone depletion or increased concentrations of greenhouse gases [Chen and Held, 2007]. See section 4.2.
6. The changes in eddy kinetic energy at upper levels are complicated by changes in jet structure, and the mean near-surface westerlies actually shift equatorward as the climate warms over part of the range of simulations. This suggests that the changes in eddy-mean flow interaction in the simulations are not straightforward and deserve further investigation.

## REFERENCES

- Adler, R. F., G. Gu, J. J. Wang, G. J. Huffman, S. Curtis, and D. Bolvin (2008), Relationships between global precipitation and surface temperature on interannual and longer timescales (1979–2006), *J. Geophys. Res.*, **113**, D22,104, doi:10.1029/2008JD010536.
- Allan, R. P., and B. J. Soden (2007), Large discrepancy between observed and simulated precipitation trends in the ascending and descending branches of the tropical circulation, *Geophys. Res. Lett.*, **34**, L18,705, doi:10.1029/2007GL031460.
- Allen, M. R., and W. J. Ingram (2002), Constraints on future changes in climate and the hydrologic cycle, *Nature*, **419**, 224–232.
- Arakawa, A., and W. H. Schubert (1974), Interaction of a cumulus cloud ensemble with the large-scale environment. Part I, *J. Atmos. Sci.*, **31**, 674–701.
- Bannon, P. R. (1986), Linear development of quasi-geostrophic baroclinic disturbances with condensational heating, *J. Atmos. Sci.*, **43**, 2261–2274.
- Becker, E., and G. Schmitz (2001), Interaction between extratropical stationary waves and the zonal mean circulation, *J. Atmos. Sci.*, **58**, 462–480.
- Bengtsson, L., K. I. Hodges, and E. Roeckner (2006), Storm tracks and climate change, *J. Climate*, **19**, 3518–3543.
- Bengtsson, L., K. I. Hodges, and N. Keenlyside (2009), Will extratropical storms intensify in a warmer climate?, *J. Climate*, **22**, 2276–2301.
- Betts, A. K. (1986), A new convective adjustment scheme. Part I: Observational and theoretical basis, *Quart. J. Roy. Meteor. Soc.*, **112**, 677–691.
- Betts, A. K. (1998), Climate-convection feedbacks: Some further issues, *Climatic Change*, **39**, 35–38.
- Betts, A. K., and Harshvardhan (1987), Thermodynamic constraint on the cloud liquid water feedback in climate models, *J. Geophys. Res.*, **92**, 8483–8485.

- Betts, A. K., and M. J. Miller (1986), A new convective adjustment scheme. Part II: Single column tests using GATE wave, BOMEX, ATEX and arctic air-mass data sets, *Quart. J. Roy. Meteor. Soc.*, **112**, 693–709.
- Betts, A. K., and M. J. Miller (1993), The Betts–Miller scheme, in *The Representation of Cumulus Convection in Numerical Models, Meteorological Monographs*, vol. 24, edited by K. A. Emanuel and D. J. Raymond, pp. 107–121, Am. Meteor. Soc.
- Betts, A. K., and W. L. Ridgway (1989), Climatic equilibrium of the atmospheric convective boundary layer over a tropical ocean, *J. Atmos. Sci.*, **46**, 2621–2641.
- Boer, G. J. (1993), Climate change and the regulation of the surface moisture and energy budgets, *Clim. Dyn.*, **8**, 225–239.
- Bordoni, S., and T. Schneider (2008), Monsoons as eddy-mediated regime transitions of the tropical overturning circulation, *Nature Geosci.*, **1**, 515–519.
- Bosilovich, M. G., S. D. Schubert, and G. K. Walker (2005), Global changes of the water cycle intensity, *J. Climate*, **18**, 1591–1608.
- Brayshaw, D. J., B. Hoskins, and M. Blackburn (2008), The storm-track response to idealized SST perturbations in an aquaplanet GCM, *J. Atmos. Sci.*, **65**, 2842–2860.
- Caballero, R. (2007), Role of eddies in the interannual variability of Hadley cell strength, *Geophys. Res. Lett.*, **34**, L18,709, doi:10.1029/2008GL035084.
- Caballero, R. (2008), Hadley cell bias in climate models linked to extratropical eddy stress, *Geophys. Res. Lett.*, **34**, L22,705, doi:10.1029/2007GL030971.
- Caballero, R., and P. L. Langen (2005), The dynamic range of poleward energy transport in an atmospheric general circulation model, *Geophys. Res. Lett.*, **32**, L02,705, doi:10.1029/2004GL021581.
- Caballero, R., R. Pierrehumbert, and J. Mitchell (2008), Axisymmetric, nearly inviscid circulations in non-condensing radiative-convective atmospheres, *Quart. J. Roy. Meteor. Soc.*, **134**, 1269–1285.
- Chang, E. K. M., S. Lee, and K. L. Swanson (2002), Storm track dynamics, *J. Climate*, **15**, 2163–2183.
- Charney, J. G. (1947), The dynamics of long waves in a baroclinic westerly current, *J. Meteor.*, **4**, 135–163.
- Chen, G., and I. M. Held (2007), Phase speed spectra and the recent poleward shift of Southern Hemisphere surface westerlies, *Geophys. Res. Lett.*, **34**, L21,805, doi:10.1029/2007GL031200.
- Chou, C., and J. D. Neelin (2004), Mechanisms of global warming impacts on regional tropical precipitation, *J. Climate*, **17**, 2688–2701.
- Chou, C., J. D. Neelin, C.-A. Chen, and J.-Y. Tu (2009), Evaluating the “rich-get-richer” mechanism in tropical precipitation change under global warming, *J. Climate*, **22**, 1982–2005.
- Clement, A. C. (2006), The role of the ocean in the seasonal cycle of the Hadley circulation, *J. Atmos. Sci.*, **63**, 3351–3365.
- Defant, A. (1921), Die Zirkulation der Atmosphäre in den gemässigten Breiten der Erde: Grundzüge einer Theorie der Klimaschwankungen, *Geograf. Ann.*, **3**, 209–266.
- Dickinson, R. E. (1971), Analytic model for zonal winds in the Tropics: I. Details of the model and simulation of gross features of the zonal mean troposphere, *Mon. Wea. Rev.*, **99**, 501–510.
- Dima, I. M., and J. M. Wallace (2003), On the seasonality of the Hadley cell, *J. Atmos. Sci.*, **60**, 1522–1527.
- Dima, I. M., J. W. Wallace, and I. Kraucunas (2005), Tropical zonal momentum balance in the NCEP reanalyses, *J. Atmos. Sci.*, **62**, 2499–2513.
- Eady, E. T. (1949), Long waves and cyclone waves, *Tellus*, **1**, 33–52.
- Edmon, H. J., B. J. Hoskins, and M. E. McIntyre (1980), Eliassen–Palm cross sections for the troposphere, *J. Atmos. Sci.*, **37**, 2600–2616.
- Emanuel, K. (2007), Quasi-equilibrium dynamics of the tropical atmosphere, in *The Global Circulation of the Atmosphere*, edited by T. Schneider and A. H. Sobel, pp. 186–218, Princeton University Press, Princeton, NJ.
- Emanuel, K. A. (1988), Observational evidence of slantwise convective adjustment, *Mon. Wea. Rev.*, **116**, 1805–1816.
- Emanuel, K. A. (1995), On thermally direct circulations in moist atmospheres, *J. Atmos. Sci.*, **52**, 1529–1534.
- Emanuel, K. A., M. Fantini, and A. J. Thorpe (1987), Baroclinic instability in an environment of small stability to slantwise moist convection. Part I: Two-dimensional models, *J. Atmos. Sci.*, **44**, 1559–1573.
- Emanuel, K. A., J. D. Neelin, and C. S. Bretherton (1994), On large-scale circulations in convecting atmospheres, *Quart. J. Roy. Meteor. Soc.*, **120**, 1111–1143.
- Fang, M., and K. K. Tung (1994), Solution to the Charney problem of viscous symmetric circulation, *J. Atmos. Sci.*, **51**, 1261–1272.
- Folkens, I., and C. Braun (2003), Tropical rainfall and boundary layer moist entropy, *J. Climate*, **16**, 1807–1820.
- Frierson, D. M. W. (2007), The dynamics of idealized convection schemes and their effect on the zonally averaged tropical circulation, *J. Atmos. Sci.*, **64**, 1959–1976.
- Frierson, D. M. W. (2008), Midlatitude static stability in simple and comprehensive general circulation models, *J. Atmos. Sci.*, **65**, 1049–1062.
- Frierson, D. M. W., I. M. Held, and P. Zurita-Gotor (2006), A gray-radiation aquaplanet moist GCM. Part I: Static stability and eddy scale, *J. Atmos. Sci.*, **63**, 2548–2566.
- Frierson, D. M. W., I. M. Held, and P. Zurita-Gotor (2007a), A gray-radiation aquaplanet moist GCM. Part II: Energy transports in altered climates, *J. Atmos. Sci.*, **64**, 1680–1693.
- Frierson, D. M. W., J. Lu, and G. Chen (2007b), Width of the Hadley cell in simple and comprehensive general circulation models, *Geophys. Res. Lett.*, **34**, L18,804, doi:10.1029/2007GL031115.
- Geng, Q., and M. Sugi (2003), Possible change of extratropical cyclone activity due to enhanced greenhouse gases and sulfate aerosols—Study with a high-resolution AGCM, *J. Climate*, **16**, 2262–2274.
- Graham, N. E., and T. P. Barnett (1987), Sea surface temperature, surface wind divergence, and convection over tropical oceans, *Science*, **238**, 657–659.
- Gu, G., R. F. Adler, G. J. Huffman, and S. Curtis (2007), Tropical rainfall variability on interannual-to-interdecadal and longer time scales derived from the GPCP monthly product, *J. Climate*, **20**, 4033–4046.
- Gutowski, W. J., Jr., L. E. Branscome, and D. A. Stewart (1992), Life cycles of moist baroclinic eddies, *J. Atmos. Sci.*, **49**, 306–319.
- Held, I. M. (1975), Momentum transport by quasi-geostrophic eddies, *J. Atmos. Sci.*, **32**, 1494–1497.
- Held, I. M. (1978), The vertical scale of an unstable baroclinic wave and its importance for eddy heat flux parameterizations, *J. Atmos. Sci.*, **35**, 572–576.
- Held, I. M. (1982), On the height of the tropopause and the static stability of the troposphere, *J. Atmos. Sci.*, **39**, 412–417.
- Held, I. M. (2000), The general circulation of the atmosphere, in *Proc. Program in Geophysical Fluid Dynamics*, Woods Hole Oceanographic Institution, Woods Hole, MA.
- Held, I. M. (2001), The partitioning of the poleward energy transport between the tropical ocean and atmosphere, *J. Atmos. Sci.*, **58**, 943–948.
- Held, I. M., and A. Y. Hou (1980), Nonlinear axially symmetric circulations in a nearly inviscid atmosphere, *J. Atmos. Sci.*, **37**, 515–533.
- Held, I. M., and B. J. Soden (2000), Water vapor feedback and global warming, *Annu. Rev. Energy Environ.*, **25**, 441–475.
- Held, I. M., and B. J. Soden (2006), Robust responses of the hydrological cycle to global warming, *J. Climate*, **19**, 5686–5699.
- Herweijer, C., R. Seager, M. Winton, and A. Clement (2005), Why ocean heat transport warms the global mean climate, *Tellus*, **57A**, 662–675.
- Hide, R. (1969), Dynamics of the atmospheres of the major planets with an appendix on the viscous boundary layer at the rigid bounding surface of an electrically-conducting rotating fluid in the presence of a magnetic field, *J. Atmos. Sci.*, **26**, 841–853.

- Hoffman, P. F., A. J. Kaufman, G. P. Halverson, and D. P. Schrag (1998), A Neoproterozoic snowball Earth, *Science*, **281**, 1342–1346.
- Hoskins, B. J., and P. J. Valdes (1990), On the existence of storm tracks, *J. Atmos. Sci.*, **47**, 1854–1864.
- Hu, Y., and Q. Fu (2007), Observed poleward expansion of the Hadley circulation since 1979, *Atmos. Chem. Phys.*, **7**, 5229–5236.
- Iribarne, J. V., and W. L. Godson (1981), *Atmospheric Thermodynamics*, Geophysics and Astrophysics Monographs, 2nd ed., 275 pp., D. Reidel, Dordrecht, Holland.
- Jeffreys, H. (1926), On the dynamics of geostrophic winds, *Quart. J. Roy. Meteor. Soc.*, **52**, 85–104.
- Johanson, C. M., and Q. Fu (2009), Hadley cell widening: Model simulations versus observations, *J. Climate*, **22**, 2713–2725.
- Juckes, M. N. (2000), The static stability of the midlatitude troposphere: The relevance of moisture, *J. Atmos. Sci.*, **57**, 3050–3057.
- Kållberg, P., A. Simmons, S. Uppala, and M. Fuentes (2004), The ERA-40 archive, *Tech. rep.*, European Centre for Medium-Range Weather Forecasts, Reading, United Kingdom.
- Kiehl, J. T., and K. E. Trenberth (1997), Earth's annual global mean energy budget, *Bull. Amer. Meteor. Soc.*, **78**, 197–208.
- Kim, H. K., and S. Y. Lee (2001), Hadley cell dynamics in a primitive equation model. Part II: Nonaxisymmetric flow, *J. Atmos. Sci.*, **58**, 2859–2871.
- Klinger, B. A., and J. Marotzke (2000), Meridional heat transport by the subtropical cell, *J. Phys. Oceanogr.*, **30**, 696–705.
- Knutson, T. R., and S. Manabe (1995), Time-mean response over the tropical Pacific to increased CO<sub>2</sub> in a coupled ocean-atmosphere model, *J. Climate*, **8**, 2181–2199.
- Korty, R. L., and K. A. Emanuel (2007), The dynamic response of the winter stratosphere to an equable climate surface temperature gradient, *J. Climate*, **20**, 5213–5228.
- Korty, R. L., and T. Schneider (2007), A climatology of the tropospheric thermal stratification using saturation potential vorticity, *J. Climate*, **20**, 5977–5991.
- Korty, R. L., and T. Schneider (2008), Extent of Hadley circulations in dry atmospheres, *Geophys. Res. Lett.*, **35**, L23,803, doi:10.1029/2008GL035847.
- Kushner, P. J., I. M. Held, and T. L. Delworth (2001), Southern Hemisphere atmospheric circulation response to global warming, *J. Climate*, **14**, 2238–2249.
- Lapeyre, G., and I. M. Held (2004), The role of moisture in the dynamics and energetics of turbulent baroclinic eddies, *J. Atmos. Sci.*, **61**, 1693–1710.
- Lee, M. I., M. J. Suarez, I. S. Kang, I. M. Held, and D. Kim (2008), A moist benchmark calculation for atmospheric general circulation models, *J. Climate*, **21**, 4934–4954.
- Levine, X. J., and T. Schneider (2009), Response of the Hadley circulation to climate change in an aquaplanet GCM coupled to ocean heat transport, *J. Atmos. Sci.*, in prep.
- Li, C., and D. S. Battisti (2008), Reduced Atlantic storminess during Last Glacial Maximum: Evidence from a coupled climate model, *J. Climate*, **21**, 3561–3579.
- Lindzen, R. S., and B. Farrell (1980), A simple approximate result for the maximum growth rate of baroclinic instabilities, *J. Atmos. Sci.*, **37**, 1648–1654.
- Lorenz, D. J., and E. T. DeWeaver (2007), The response of the extratropical hydrological cycle to global warming, *J. Climate*, **20**, 3470–3484.
- Lorenz, E. N. (1955), Available potential energy and the maintenance of the general circulation, *Tellus*, **7**, 157–167.
- Lorenz, E. N. (1978), Available energy and the maintenance of a moist circulation, *Tellus*, **30**, 15–31.
- Lorenz, E. N. (1979), Numerical evaluation of moist available energy, *Tellus*, **31**, 230–235.
- Lu, J., G. A. Vecchi, and T. Reichler (2007), Expansion of the Hadley cell under global warming, *Geophys. Res. Lett.*, **34**, L06,805, doi:10.1029/2006GL028443.
- Neelin, J. D. (2007), Moist dynamics of tropical convection zones in monsoons, teleconnections, and global warming, in *The Global Circulation of the Atmosphere*, edited by T. Schneider and A. H. Sobel, chap. 10, pp. 267–301, Princeton University Press, Princeton, NJ.
- Neelin, J. D., C. Chou, and H. Su (2003), Tropical drought regions in global warming and El Niño teleconnections, *Geophys. Res. Lett.*, **30**, 2275, doi:10.1029/2003GL018625.
- Neelin, J. D., M. Münnich, H. Su, J. E. Meyerson, and C. E. Holloway (2006), Tropical drying trends in global warming models and observations, *Proc. Nat. Acad. Sci.*, **103**, 6110–6115.
- Neelin, J. D., O. Peters, J. W.-B. Lin, K. Hales, and C. E. Holloway (2008), Rethinking convective quasi-equilibrium: observational constraints for stochastic convective schemes in climate models, *Phil. Trans. Roy. Soc. A*, **366**, 2581–2604.
- Neelin, J. D., O. Peters, and K. Hales (2009), The transition to strong convection, *J. Atmos. Sci.*, **66**, 2367–2384.
- O’Gorman, P. A., and T. Schneider (2006), Stochastic models for the kinematics of moisture transport and condensation in homogeneous turbulent flows, *J. Atmos. Sci.*, **63**, 2992–3005.
- O’Gorman, P. A., and T. Schneider (2008a), The hydrological cycle over a wide range of climates simulated with an idealized GCM, *J. Climate*, **21**, 3815–3832.
- O’Gorman, P. A., and T. Schneider (2008b), Energy of midlatitude transient eddies in idealized simulations of changed climates, *J. Climate*, **21**, 5797–5806.
- O’Gorman, P. A., and T. Schneider (2009a), Scaling of precipitation extremes over a wide range of climates simulated with an idealized GCM, *J. Climate*, **22**, 5676–5685.
- O’Gorman, P. A., and T. Schneider (2009b), The physical basis for increases in precipitation extremes in simulations of 21st-century climate change, *Proc. Nat. Acad. Sci.*, **106**, 14,773–14,777.
- Orlanski, I. (1998), Poleward deflection of storm tracks, *J. Atmos. Sci.*, **55**, 2577–2602.
- Otto-Bliesner, B. L., and A. Clement (2005), The sensitivity of the Hadley circulation to past and future forcings in two climate models, in *The Hadley Circulation: Present, Past and Future*, edited by H. F. Diaz and R. S. Bradley, pp. 437–464, Kluwer Academic Publishers, Netherlands.
- Peixoto, J. P., and A. H. Oort (1992), *Physics of Climate*, 555 pp., American Institute of Physics.
- Pierrehumbert, R. T. (2002), The hydrologic cycle in deep-time climate problems, *Nature*, **419**, 191–198.
- Pierrehumbert, R. T., H. Brogniez, and R. Roca (2007), On the relative humidity of the atmosphere, in *The Global Circulation of the Atmosphere*, edited by T. Schneider and A. H. Sobel, pp. 143–185, Princeton University Press, Princeton, NJ.
- Previdi, M., and B. G. Liepert (2007), Annular modes and Hadley cell expansion under global warming, *Geophys. Res. Lett.*, **34**, L22,701, doi:10.1029/2007GL031243.
- Reed, R. J., A. J. Simmons, M. D. Albright, and P. Undén (1988), The role of latent heat release in explosive cyclogenesis: Three examples based on ECMWF operational forecasts, *Wea. Forecast.*, **3**, 217–229.
- Rind, D. (1986), The dynamics of warm and cold climates, *J. Atmos. Sci.*, **43**, 3–25.
- Roads, J., S. C. Chen, S. Marshall, and R. Oglesby (1998), Atmospheric moisture cycling rate trends from model runs, *GEWEX News*, **8**, 1, 7–10.
- Santer, B. D., et al. (2003a), Behavior of tropopause height and atmospheric temperature in models, reanalyses, and observations: Decadal changes, *J. Geophys. Res.*, **108D**, 4002, doi:10.1029/2002JD002258.
- Santer, B. D., et al. (2003b), Contributions of anthropogenic and natural forcing to recent tropopause height changes, *Science*, **301**, 479–483.
- Schneider, E. K. (1977), Axially symmetric steady-state models of the basic state for instability and climate studies. Part II. Nonlinear calculations, *J. Atmos. Sci.*, **34**, 280–296.
- Schneider, E. K. (1981), On the amplitudes reached by baroclinically unstable disturbances, *J. Atmos. Sci.*, **38**, 2142–2149.

- Schneider, E. K. (1984), Response of the annual and zonal mean winds and temperatures to variations in the heat and momentum sources, *J. Atmos. Sci.*, **41**, 1093–1115.
- Schneider, E. K., and R. S. Lindzen (1977), Axially symmetric steady-state models of the basic state for instability and climate studies. Part I. Linearized calculations, *J. Atmos. Sci.*, **34**, 263–279.
- Schneider, T. (2006), The general circulation of the atmosphere, *Ann. Rev. Earth Planet. Sci.*, **34**, 655–688.
- Schneider, T. (2007), The thermal stratification of the extratropical troposphere, in *The Global Circulation of the Atmosphere*, edited by T. Schneider and A. H. Sobel, pp. 47–77, Princeton University Press, Princeton, NJ.
- Schneider, T., and S. Bordoni (2008), Eddy-mediated regime transitions in the seasonal cycle of a Hadley circulation and implications for monsoon dynamics, *J. Atmos. Sci.*, **65**, 915–934.
- Schneider, T., and P. A. O’Gorman (2007), Precipitation and its extremes in changed climates, in *Extreme Events*, edited by P. Müller, C. Garrett, and D. Henderson, Proceedings ‘Aha Huli’ a Hawaiian Winter Workshop, pp. 61–66, University of Hawaii at Manoa, Honolulu, HI.
- Schneider, T., and P. A. O’Gorman (2008), Moist convection and the thermal stratification of the extratropical troposphere, *J. Atmos. Sci.*, **65**, 3571–3583.
- Schneider, T., and C. C. Walker (2006), Self-organization of atmospheric macroturbulence into critical states of weak nonlinear eddy–eddy interactions, *J. Atmos. Sci.*, **63**, 1569–1586.
- Schneider, T., and C. C. Walker (2008), Scaling laws and regime transitions of macroturbulence in dry atmospheres, *J. Atmos. Sci.*, **65**, 2153–2173.
- Seidel, D. J., and W. J. Randel (2007), Recent widening of the tropical belt: Evidence from tropopause observations, *J. Geophys. Res.*, **112**, D20,113.
- Seidel, D. J., R. J. Ross, J. K. Angell, and G. C. Reid (2001), Climatological characteristics of the tropical tropopause as revealed by radiosondes, *J. Geophys. Res.*, **106**, 7857–7878.
- Seidel, D. J., Q. Fu, W. J. Randel, and T. J. Reichler (2008), Widening of the tropical belt in a changing climate, *Nature Geosci.*, **1**, 21–24.
- Sherwood, S. C., R. Roca, T. M. Weckwerth, and N. G. Andronova (2009), Tropospheric water vapor, convection and climate: a critical review, *Rev. Geophys.*, in press.
- Simmons, A. J., and B. J. Hoskins (1978), The life cycles of some nonlinear baroclinic waves, *J. Atmos. Sci.*, **35**, 414–432.
- Simmons, A. J., A. Untch, C. Jakob, P. Kållberg, and P. Undén (1999), Stratospheric water vapour and tropical tropopause temperatures in ECMWF analyses and multi-year simulations, *Quart. J. Roy. Meteor. Soc.*, **125**, 353–386.
- Sobel, A. H., and T. Schneider (2009), Single-layer axisymmetric model for a Hadley circulation with parameterized eddy momentum forcing, *J. Adv. Model. Earth Sys.*, pp. Art. #10, 11 pp., doi:10.3894/JAMES.2009.1.10.
- Stephens, G. L., and T. D. Ellis (2008), Controls of global-mean precipitation increases in global warming GCM experiments, *J. Climate*, **21**, 6141–6155.
- Tanaka, H. L., N. Ishizaki, and A. Kitoh (2004), Trend and interannual variability of Walker, monsoon and Hadley circulations defined by velocity potential in the upper troposphere, *Tellus*, **56A**, 250–269.
- Thuburn, J., and G. C. Craig (2000), Stratospheric influence on tropopause height: The radiative constraint, *J. Atmos. Sci.*, **57**, 17–28.
- Trenberth, K., and J. Caron (2001), Estimates of meridional atmosphere and ocean heat transports, *J. Climate*, **14**, 3433–3443.
- Trenberth, K. E., and L. Smith (2005), The mass of the atmosphere: A constraint on global analyses, *J. Climate*, **18**, 864–875.
- Trenberth, K. E., and D. P. Stepaniak (2003a), Seamless poleward atmospheric energy transports and implications for the Hadley circulation, *J. Climate*, **16**, 3706–3722.
- Trenberth, K. E., and D. P. Stepaniak (2003b), Covariability of components of poleward atmospheric energy transports on seasonal and interannual timescales, *J. Climate*, **16**, 3691–3705.
- Trenberth, K. E., A. Dai, R. M. Rasmussen, and D. B. Parsons (2003), The changing character of precipitation, *Bull. Amer. Meteor. Soc.*, **84**, 1205–1217.
- Trenberth, K. E., J. Fasullo, and L. Smith (2005), Trends and variability in column-integrated atmospheric water vapor, *Climate Dyn.*, **24**, 741–758.
- Trenberth, K. E., J. T. Fasullo, and J. Kiehl (2009), Earth’s global energy budget, *Bull. Amer. Meteor. Soc.*, **90**, 311–323.
- Uppala, S. M., et al. (2005), The ERA-40 reanalysis, *Quart. J. Roy. Meteor. Soc.*, **131**, 2961–3012.
- Vecchi, G. A., and B. J. Soden (2007), Global warming and the weakening of the tropical circulation, *J. Climate*, **20**, 4316–4340.
- Vecchi, G. A., B. J. Soden, A. T. Wittenberg, I. M. Held, A. Leetmaa, and M. J. Harrison (2006), Weakening of tropical Pacific atmospheric circulation due to anthropogenic forcing, *Nature*, **441**, 73–76.
- Walker, C. C., and T. Schneider (2005), Response of idealized Hadley circulations to seasonally varying heating, *Geophys. Res. Lett.*, **32**, L06,813, doi:10.1029/2004GL022304.
- Walker, C. C., and T. Schneider (2006), Eddy influences on Hadley circulations: Simulations with an idealized GCM, *J. Atmos. Sci.*, **63**, 3333–3350.
- Wentz, F. J., and M. Schabel (2000), Precise climate monitoring using complementary satellite data sets, *Nature*, **403**, 414–416.
- Wentz, F. J., L. Ricciardulli, K. Hilburn, and C. Mears (2007), How much more rain will global warming bring?, *Science*, **317**, 233–235.
- Wernli, H., S. Dirren, M. A. Liniger, and M. Zillig (2002), Dynamical aspects of the life cycle of the winter storm ‘Lothar’ (24–26 December 1999), *Quart. J. Roy. Meteor. Soc.*, **128**, 405–429.
- Willett, K. M., N. P. Gillett, P. D. Jones, and P. W. Thorne (2007), Attribution of observed surface humidity changes to human influence, *Nature*, **449**, 710–713.
- Yin, J. H. (2005), A consistent poleward shift of the storm tracks in simulations of 21st century climate, *Geophys. Res. Lett.*, **32**, L18,701, doi:10.1029/2005GL023684.
- Zhang, M., and H. Song (2006), Evidence of deceleration of atmospheric vertical overturning circulation over the tropical Pacific, *Geophys. Res. Lett.*, **33**, L12,701, doi:10.1029/2006GL025942.
- Zurita-Gotor, P. (2005), Updraft/downdraft constraints for moist baroclinic modes and their implications for the short-wave cut-off and maximum growth rate, *J. Atmos. Sci.*, **62**, 4450–4458.

Tapio Schneider, California Institute of Technology, Pasadena, CA 91125-2300, USA. (tapio@caltech.edu)  
 Paul A. O’Gorman, Massachusetts Institute of Technology, Cambridge, MA 02139, USA. (pog@mit.edu)  
 Xavier J. Levine, California Institute of Technology, Pasadena, CA 91125-2300, USA. (xavier@caltech.edu)